
Temperature Effect on Stress Concentration Around Circular Hole in a Composite Material Specimen Representative of X-29A Forward- Swept Wing Aircraft

Hsien-Yang Yeh

Mechanical Engineering Department, California State University, Long Beach, Long Beach, California 90840

Prepared for
Ames Research Center
Dryden Flight Research Facility
Edwards, California
under contract NGT 05020412

1988



National Aeronautics and
Space Administration

Ames Research Center

Dryden Flight Research Facility
Edwards, California 93523-5000

Temperature Effect on Stress Concentration Around Circular Hole in a Composite Material Specimen Representative of X-29A Forward-Swept Wing Aircraft

Hsien-Yang Yeh
Mechanical Engineering Department
California State University, Long Beach

SUMMARY

The theory of anisotropic elasticity was used to evaluate the anisotropic stress concentration factors of a composite laminated plate containing a small circular hole. This advanced composite material was used to manufacture the X-29A forward-swept wing. Observe that the usual isotropic material stress concentration factor is three. It was found that for composite material, the anisotropic stress concentration factor is no longer a constant, and that the locations of maximum tangential stress points could shift by changing the fiber orientation with respect to the loading axis. The analysis showed that through the lamination process, the stress concentration factor could be reduced drastically, and therefore the structural performance could be improved. Both the mixture rule approach and the constant strain approach were used to calculate the stress concentration factor of room temperature. The results predicted by the mixture rule approach were about twenty percent deviate from the experimental data. However, the results predicted by the constant strain approach matched the testing data very well. This showed the importance of the inplane shear effect on the evaluation of stress concentration factor for the X-29A composite plate.

At low temperature (-60°F), the results predicted by the mixture rule approach provided good correlation with the experimental data. At elevated temperature (200°F), the results calculated from the constant strain approach were about ten percent conservative than the experimental data. These showed both the advantages and the limitations of different analytical models in predicting stress concentration factors at various temperature levels. Furthermore, the experimental data showed the stress concentration factors decreased as the temperature increased.

ACKNOWLEDGEMENTS

This work was supported by the NASA-ASEE Summer Faculty Fellowship in 1988. The author is greatly indebted to Donald C. Bacon, Jr., assistant chief of research engineering division, V. Michael DeAngelis, branch chief of aerostructures, Don Black, deputy branch chief of aerostructures, Lawrence F. Reardon, group leader of structural test operation and Dr. William L. Ko, aerospace engineer for invaluable advice, experimental data collection and helpful discussions.

INTRODUCTION

The X-29A advanced technology demonstrator is sponsored by the Defense Advanced Research Projects Agency with support from NASA and the Air Force.

The X-29A features a unique forward-swept wing (Fig. 1), made of composite materials which offers weight reduction of as much as 20 percent in comparison with convention aft-swept wings.

A forward-swept wing is prone to structural divergence, because as dynamic pressure increases, forces tend to bend the leading edge up. If a divergent speed were reached, a cycle of leading edge bending, increased local angle of attack and greater wing loading could grow to cause a structural failure. The wing's high rigidity prevents divergence from occurring within the X-29A's flight envelope.

Because of their importance in aircraft design application, laminated, continuous-fiber reinforced-resin matrix composites containing through cutouts have been the subject of considerable study (refs. 1 to 6). In this paper, anisotropic plate theory was used to calculate the anisotropic stress concentration factors (SCF) for the X-29A composite plate containing a circular hole.

NOMENCLATURE

A_{ij}	equivalent modulus or extensional stiffness for a multidirectional laminate
E_1	modulus of elasticity of anisotropic plate in axis-1 direction
E_2	modulus of elasticity of anisotropic plate in axis-2 direction
\bar{E}_1	modulus of elasticity of laminated composite plate in axis-1 direction
\bar{E}_2	modulus of elasticity of laminated composite plate in axis-2 direction
$\bar{\bar{E}}_1$	transformed modulus of elasticity of single-ply in axis-1 direction
$\bar{\bar{E}}_2$	transformed modulus of elasticity of single-ply in axis-2 direction
E_α	modulus of elasticity of anisotropic plate in α direction
E_L	modulus of elasticity of single-ply to fiber direction
E_T	modulus of elasticity of single-ply transverse in fiber direction
G_{12}	shear modulus of anisotropic plate associated with $\{1, 2\}$ coordinate system
\bar{G}_{12}	shear modulus of laminated composite plate associated with $\{1, 2\}$ coordinate system
$\bar{\bar{G}}_{12}$	transformed shear modulus of single-ply in $\{1, 2\}$ coordinate system
G_{LT}	shear modulus of single-ply associated with $\{L, T\}$ coordinate system
K	stress concentration factor
k	$\sqrt{\frac{E_1}{E_2}}$
N_i	stress resultant
Q_{ij}	reduced stiffness of single-ply
\bar{Q}_{ij}	transformed reduced stiffness of single-ply associated with $\{1, 2\}$ coordinate system
ν_{12}	Poisson's ratio of anisotropic plate associated with $\{1, 2\}$ coordinate system
$\bar{\nu}_{12}, \bar{\nu}_{21}$	Poisson's ratios of laminated composite plate associated with $\{1, 2\}$ coordinate system
$\bar{\bar{\nu}}_{12}, \bar{\bar{\nu}}_{21}$	transformed Poisson's ratios of single-ply in $\{1, 2\}$ coordinate system
ν_{LT}	Poisson's ratio of single-ply associated with $\{L, T\}$ coordinate system

ϵ_i	constant strain
σ_α	stress in α direction
σ_∞	remote tensile stress

ANALYSIS

Let axes 1,2 be the principal coordinate axes of the laminated plate, and let axes L,T be the principal material axes of the single composite ply shown in figure 2.

For an anisotropic plate containing a circular hole subjected to remote uniaxial tensile stress σ_∞ , acting at an angle ϕ with respect to the principal elastic axis 1 of the plate (fig. 3), the tangential stress, σ_α and tangential stress concentration factor, $K \equiv \sigma_\alpha/\sigma_\phi$ along the circular hole boundary may be expressed as (ref. 3)

$$K \equiv \frac{\sigma_\alpha}{\sigma_\infty} = \frac{E_\alpha}{E_1} \{ [-\cos^2 \phi + (k+n) \sin^2 \phi] k \cos^2 \alpha + [(1+n) \cos^2 \phi - k \sin^2 \phi] \sin^2 \alpha - n(1+k+n) \sin \phi \cos \phi \sin \alpha \cos \alpha \} \quad (1)$$

where E_α is the modulus of elasticity in the α direction (fig. 3) given by

$$\frac{E_\alpha}{E_1} = 1 / \left[\sin^4 \alpha + \frac{E_1}{E_2} \cos^4 \alpha + \frac{1}{4} \left(\frac{E_1}{G_{12}} - 2\nu_{12} \right) \sin^2 2\alpha \right] \quad (2)$$

where k and n are defined by

$$k \equiv -\mu_1 \mu_2 = \sqrt{\frac{E_1}{E_2}} \quad (3)$$

$$n \equiv -i(\mu_1 + \mu_2) = \sqrt{2 \left(\sqrt{\frac{E_1}{E_2}} - \nu_{12} \right) + \frac{E_1}{G_{12}}} \quad (4)$$

where $i \equiv \sqrt{-1}$, and μ_1 and μ_2 are the complex roots of the anisotropic plate characteristic equation

$$\mu^4 + \left(\frac{E_1}{G_{12}} - 2\nu_{12} \right) \mu^2 + \frac{E_1}{E_2} = 0 \quad (5)$$

For isotropic materials $k = 1$ and $n = 2$, and the stress concentration factor K (eq. (1)) reduces to

$$K = \frac{\sigma_\alpha}{\sigma_\infty} = 1 - 2 \cos 2(\alpha - \phi) \quad (6)$$

which gives $K = -1$ at $(\alpha - \phi) = 0$ or π , and $K = 3$ at $(\alpha - \phi) = \pm\pi/2$.

To evaluate the modulus of elasticity of a laminated plate, both the mixture rule approach and the constant strain approach could be used. In the mixture rule approach, the transformed ply-elastic constants $\{\bar{E}_1, \bar{E}_2, \bar{G}_{12}, \bar{\nu}_{12}, \bar{\nu}_{21}\}$

with respect to the $\{1, 2\}$ system can be related to the material constants $\{E_L, E_T, G_{LT}, \nu_{LT}, \nu_{TL}\}$ with respect to the $\{L, T\}$ system through the following equations (refs. 6 and 7).

$$\begin{aligned}
 \bar{\bar{E}}_1 &= E_L / \left[\cos^4 \Theta + \frac{E_L}{E_T} \sin^4 \Theta + \frac{1}{4} \left(\frac{E_L}{G_{LT}} - 2\nu_{LT} \right) \sin^2 2\Theta \right] \\
 \bar{\bar{E}}_2 &= E_L / \left[\sin^4 \Theta + \frac{E_L}{E_T} \cos^4 \Theta + \frac{1}{4} \left(\frac{E_L}{G_{LT}} - 2\nu_{LT} \right) \sin^2 2\Theta \right] \\
 \bar{\bar{G}}_{12} &= E_L / \left[1 + 2\nu_{LT} + \frac{E_L}{E_T} - \left(1 + 2\nu_{LT} + \frac{E_L}{E_T} - \frac{E_L}{G_{LT}} \right) \cos^2 2\Theta \right] \\
 \bar{\bar{\nu}}_{12} &= \frac{E_1}{E_L} \left[\nu_{LT} - \frac{1}{4} \left(1 + 2\nu_{LT} + \frac{E_L}{E_T} - \frac{E_L}{G_{LT}} \right) \sin^2 2\Theta \right] \\
 \bar{\bar{\nu}}_{21} &= \frac{E_2}{E_L} \left[\nu_{LT} - \frac{1}{4} \left(1 + 2\nu_{LT} + \frac{E_L}{E_T} - \frac{E_L}{G_{LT}} \right) \sin^2 2\Theta \right]
 \end{aligned} \tag{7}$$

If the composite plate is made of N number of single plies with different fiber orientations, then by using the mixture rule, the engineering elastic constants $\{\bar{E}_1, \bar{E}_2, \bar{G}_{12}, \bar{\nu}_{12}, \bar{\nu}_{21}\}$ for the composite plate can be written as

$$\begin{aligned}
 \bar{E}_1 &= \frac{1}{N} \sum_{j=1}^N \bar{\bar{E}}_1(\Theta_j) \\
 \bar{E}_2 &= \frac{1}{N} \sum_{j=1}^N \bar{\bar{E}}_2(\Theta_j) \\
 \bar{G}_{12} &= \frac{1}{N} \sum_{j=1}^N \bar{\bar{G}}_{12}(\Theta_j) \\
 \bar{\nu}_{12} &= \frac{1}{N} \sum_{j=1}^N \bar{\bar{\nu}}_{12}(\Theta_j) \\
 \bar{\nu}_{21} &= \frac{1}{N} \sum_{j=1}^N \bar{\bar{\nu}}_{21}(\Theta_j)
 \end{aligned} \tag{8}$$

In the constant strain approach, it is assumed that the strain remains constant across the laminate thickness and the inplane stress-strain relation for a laminate is used and it is actually the stress resultant versus inplane strain relation.

$$\begin{aligned}
 N_1 &= A_{11} \epsilon_1 + A_{12} \epsilon_2 + A_{16} \epsilon_6 \\
 N_2 &= A_{21} \epsilon_1 + A_{22} \epsilon_2 + A_{26} \epsilon_6 \\
 N_6 &= A_{61} \epsilon_1 + A_{62} \epsilon_2 + A_{66} \epsilon_6
 \end{aligned} \tag{9}$$

where A_{ij} are defined by (refs. 7 and 8)

$$A_{ij} = \sum_{k=1}^N (\bar{Q}_{ij})_k (z_k - z_{k-1}) \quad i, j = 1, 2, 6 \tag{10}$$

in which

$$\begin{aligned}
\bar{Q}_{11} &= Q_{11} \cos^4 \theta + 2(Q_{12} + 2Q_{66}) \sin^2 \theta \cos^2 \theta + Q_{22} \sin^4 \theta \\
\bar{Q}_{12} &= (Q_{11} + Q_{22} - 4Q_{66}) \sin^2 \theta \cos^2 \theta + Q_{12}(\sin^4 \theta + \cos^4 \theta) \\
\bar{Q}_{22} &= Q_{11} \sin^4 \theta + 2(Q_{12} + 2Q_{66}) \sin^2 \theta \cos^2 \theta + Q_{22} \cos^4 \theta \\
\bar{Q}_{16} &= (Q_{11} - Q_{12} - 2Q_{66}) \sin \theta \cos^3 \theta + (Q_{12} - Q_{22} + 2Q_{66}) \sin^3 \theta \cos \theta \\
\bar{Q}_{26} &= (Q_{11} - Q_{12} - 2Q_{66}) \sin^3 \theta \cos \theta + (Q_{12} - Q_{22} + 2Q_{66}) \sin \theta \cos^3 \theta \\
\bar{Q}_{66} &= (Q_{11} + Q_{22} - 2Q_{12} - 2Q_{66}) \sin^2 \theta \cos^2 \theta + Q_{66}(\sin^4 \theta + \cos^4 \theta)
\end{aligned} \tag{11}$$

and

$$\begin{aligned}
Q_{11} &= \frac{E_L}{1 - \nu_{LT}\nu_{TL}} \\
Q_{12} &= \frac{\nu_{LT}E_T}{1 - \nu_{LT}\nu_{TL}} = \frac{\nu_{TL}E_L}{1 - \nu_{LT}\nu_{TL}} \\
Q_{22} &= \frac{E_T}{1 - \nu_{LT}\nu_{TL}} \\
Q_{66} &= G_{LT}
\end{aligned} \tag{12}$$

The calculation of the effective engineering elastic constants $\{\bar{E}_1, \bar{E}_2, \bar{G}_{12}, \bar{\nu}_{12}\}$ is performed by relating the compliance components to inplane engineering constants under uniaxial tension along the 1-axis (ref. 9).

RESULTS

The X-29A forward-swept wing composite plate is made up of 40-plyes with the total thickness of .56 cm (.22 in.). The stacking sequence and the ply-engineering elastic constants are given by

$$[\pm 45 | 0_4 | \pm 45 | 90_2 | \pm 45 | 0_4 | \pm 45 | 0_2]_s$$

-60°F	70°F	-200°F
$E_L = 19.23 \times 10^6$ psi	$E_L = 18.76 \times 10^6$ psi	$E_L = 18.29 \times 10^6$ psi
$E_T = 1.71 \times 10^6$ psi	$E_T = 1.57 \times 10^6$ psi	$E_T = 1.44 \times 10^6$ psi
$G_{LT} = 0.858 \times 10^6$ psi	$G_{LT} = 0.82 \times 10^6$ psi	$G_{LT} = 0.785 \times 10^6$ psi
$\nu_{LT} = 0.312$	$\nu_{LT} = 0.312$	$\nu_{LT} = 0.312$

By replacing $\{E_1, E_2, G_{12}, \nu_{12}\}$, respectively, with $\{\bar{E}_1, \bar{E}_2, \bar{G}_{12}, \bar{\nu}_{12}\}$ in equations (1), (2), (3), and (4), the tangential stresses σ_α around a circular hole in a laminated X-29A composite plate were calculated for three loading cases: $\phi = 0$ (loading in axis-1 direction), $\phi = \frac{\pi}{4}$, and $\phi = \frac{\pi}{2}$ (loading in axis-2 direction). The results obtained from the constant strain approach and the mixture rule approach of three different temperature levels (-60°F, 70°F, and 200°F) are plotted in figures 1 to 27 and figures 28 to 33, respectively. Figures 1, 4, and 7 show the plot of stress concentration factors around the circular hole of the laminated X-29A composite material when the plate is under uniaxial tension in the composite elastic axis-1 direction. The maximum stress concentration factor K for the laminated X-29A composite plate reached the peak value of about 4.5 (larger than 3) in three different temperature

levels at two locations ($\alpha = 90^\circ$ and $\alpha = 270^\circ$). Figures 2, 3, 5, 6, 8, and 9 show the polar coordinate plots of σ_α for the laminated X-29A composite material when the plate is under uniaxial tension in the composite elastic axis-1 direction. When the loading axis is $\phi = \frac{\pi}{4}$ oblique to the composite axis-1 (figures 10, 13, and 16), the maximum stress concentration factor K reached the peak value of 3 in three different temperature levels at four locations ($\alpha = 120^\circ, 300^\circ$ by constant strain approach and $\alpha = 105^\circ$ and 285° by mixture rule approach). Again, figures 11, 12, 14, 15, 17, and 18 show the polar coordinate plots of σ_α for the laminated X-29A composite material when the plate is under uniaxial tension and the loading axis is 45° oblique to the composite axis-1.

As the loading axis is $\phi = \frac{\pi}{2}$ perpendicular to the composite axis-1, figures 19, 22, and 25 show the maximum stress concentration K for the laminated X-29A composite plate reached the peak value of about 3 in three different temperature levels at two locations ($\alpha = 0^\circ$ and $\alpha = 180^\circ$). And figures 20, 21, 23, 24, 26, and 27 show the polar coordinate plots of σ_α for the laminated X-29A composite material when the plate is under uniaxial tension and the loading axis is 90° perpendicular to the composite axis-1.

For comparison purposes, figures 28, 30, and 32 show the correlation of the maximum stress concentration factors in polar coordinate plots at three different temperature levels. Figures 29, 31, and 33 show the variation of the maximum stress concentration factor along the boundary of the circular hole at three different temperature levels.

The stress concentration factors evaluated from different approaches (mixture rule and constant strain) discussed previously were compared by performing simple coupon tests. The width W of the rectangular specimen is 3.81 cm (1.5 in.) and the diameter of the small central circular hole is 0.635 cm (0.25 in.). The comparison of stress concentration factors between theoretical predictions and experimental results are listed in table 1.

CONCLUSION

The theory of anisotropic elasticity was used to evaluate the anisotropic stress concentration factors for laminated OBX-29A (forward-swept wing) research aircraft composite plates of three different temperature levels.

It is well known that the usual isotropic material stress concentration factor is three. However, the analysis showed that the anisotropic stress concentration factor could be greater or less than three for composite materials, and the locations of the maximum tangential stress points could shift by the change of fiber orientation with respect to the loading axis.

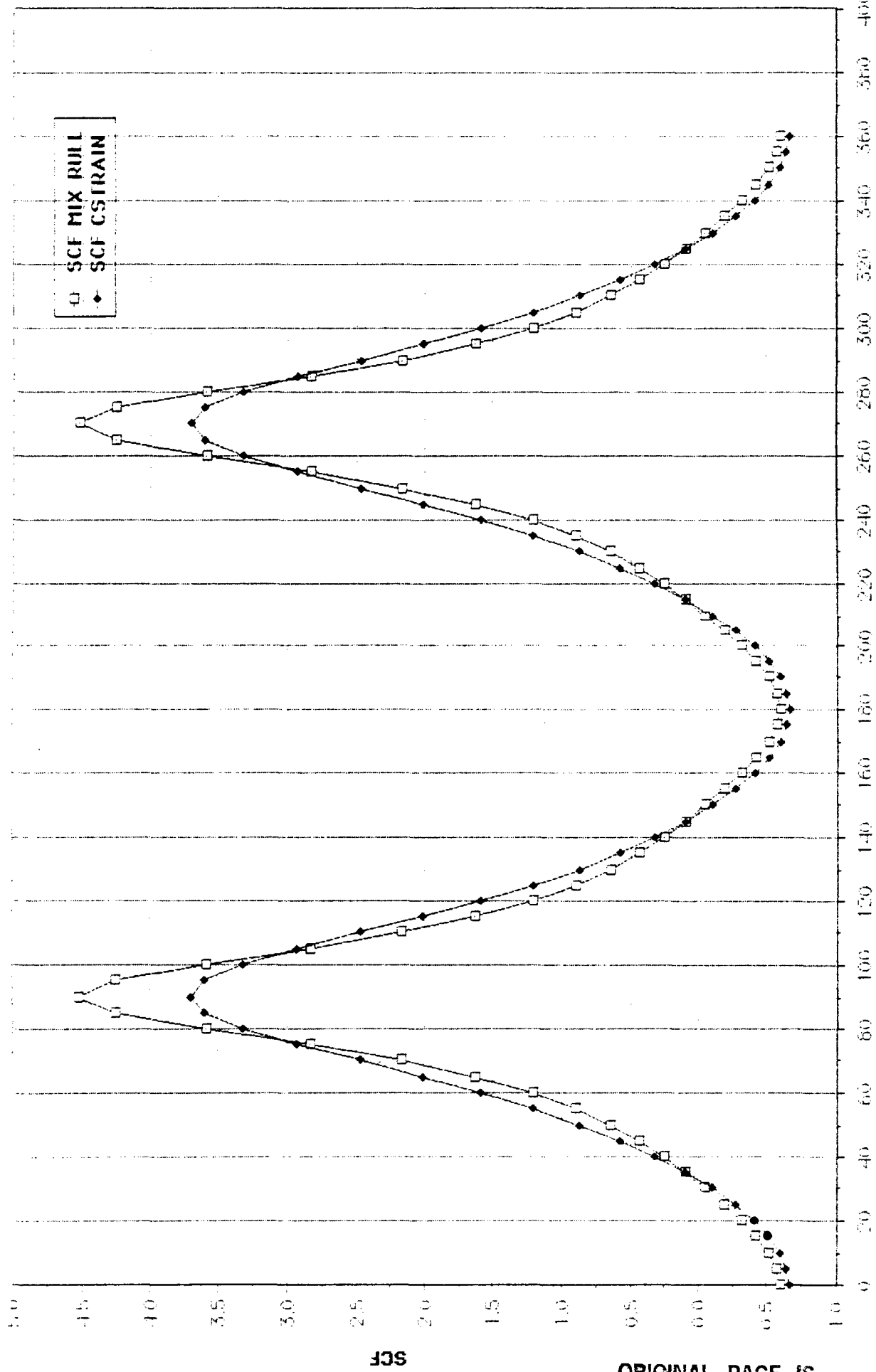
Both the mixture rule approach and the constant strain approach were used to calculate stress concentration factors of room temperature. The results obtained by the mixture rule approach were about twenty percent deviate from the experimental data. However, the results predicted by the constant strain approach matched the testing data very well. This showed the importance of the inplane shear effect on the evaluation of stress concentration factors for the laminated X-29A composite plate. A further investigation about the inplane shear effect will need a three dimensional model from anisotropic elasticity plus the interlaminar stress analysis.

At low temperature (-60°F), the results predicted by the mixture rule approach provided good correlation with the experimental data. At elevated temperature (200°F), the results calculated from the constant strain approach were about ten percent more conservative than the experimental data. These showed both the advantages and the limitations of different analytical models in predicting stress concentration factors at various temperature levels. Furthermore, the experimental data showed the stress concentration factors decreased as the temperature increased.

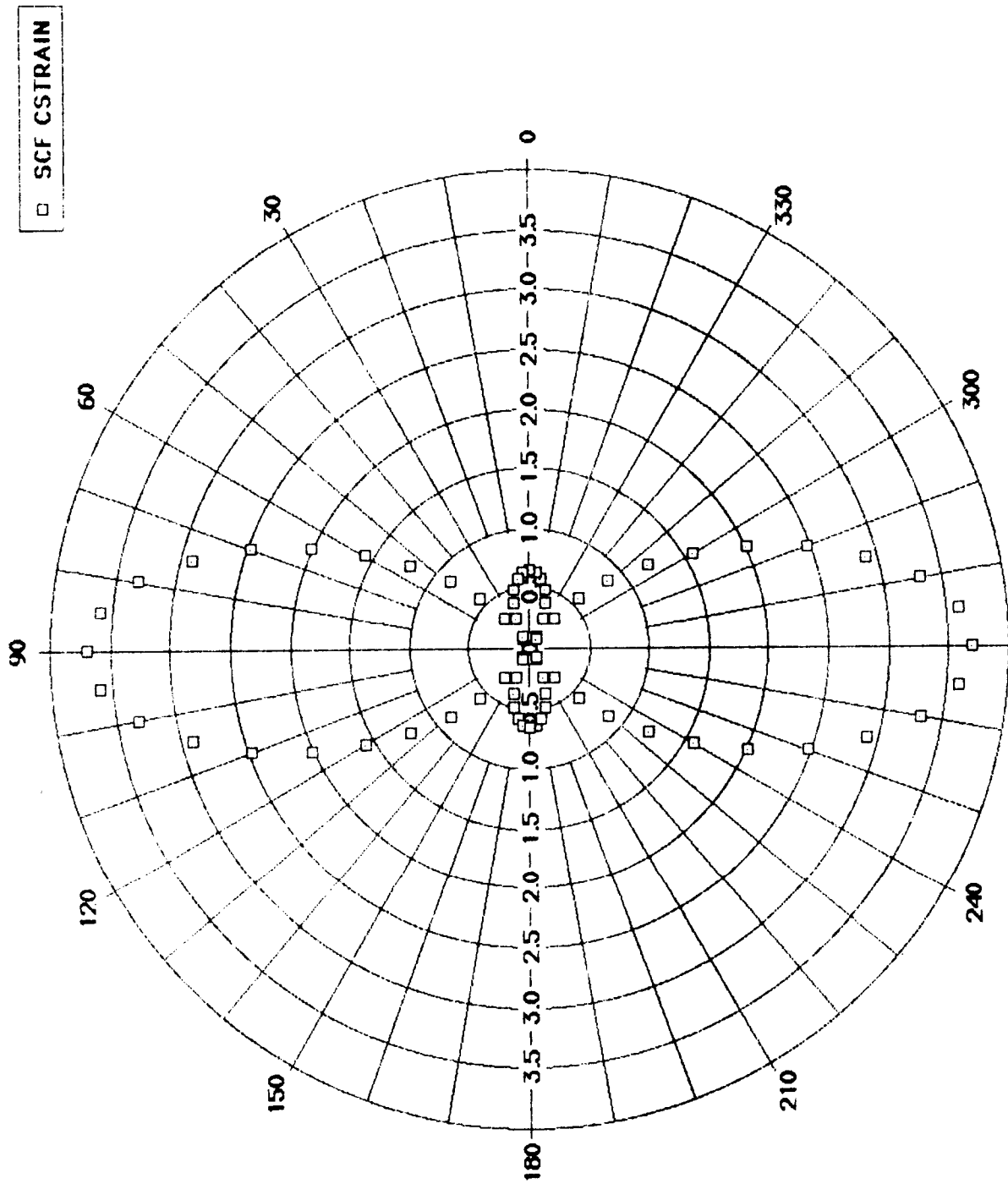
The anisotropic stress concentration of laminated plates is a difficult and complicated problem. To obtain a better understanding of this physical phenomenon, consideration of the hole size effect and utilization, the theory of linear elastic fracture mechanics, and the theory of micromechanics is imperative.

REFERENCES

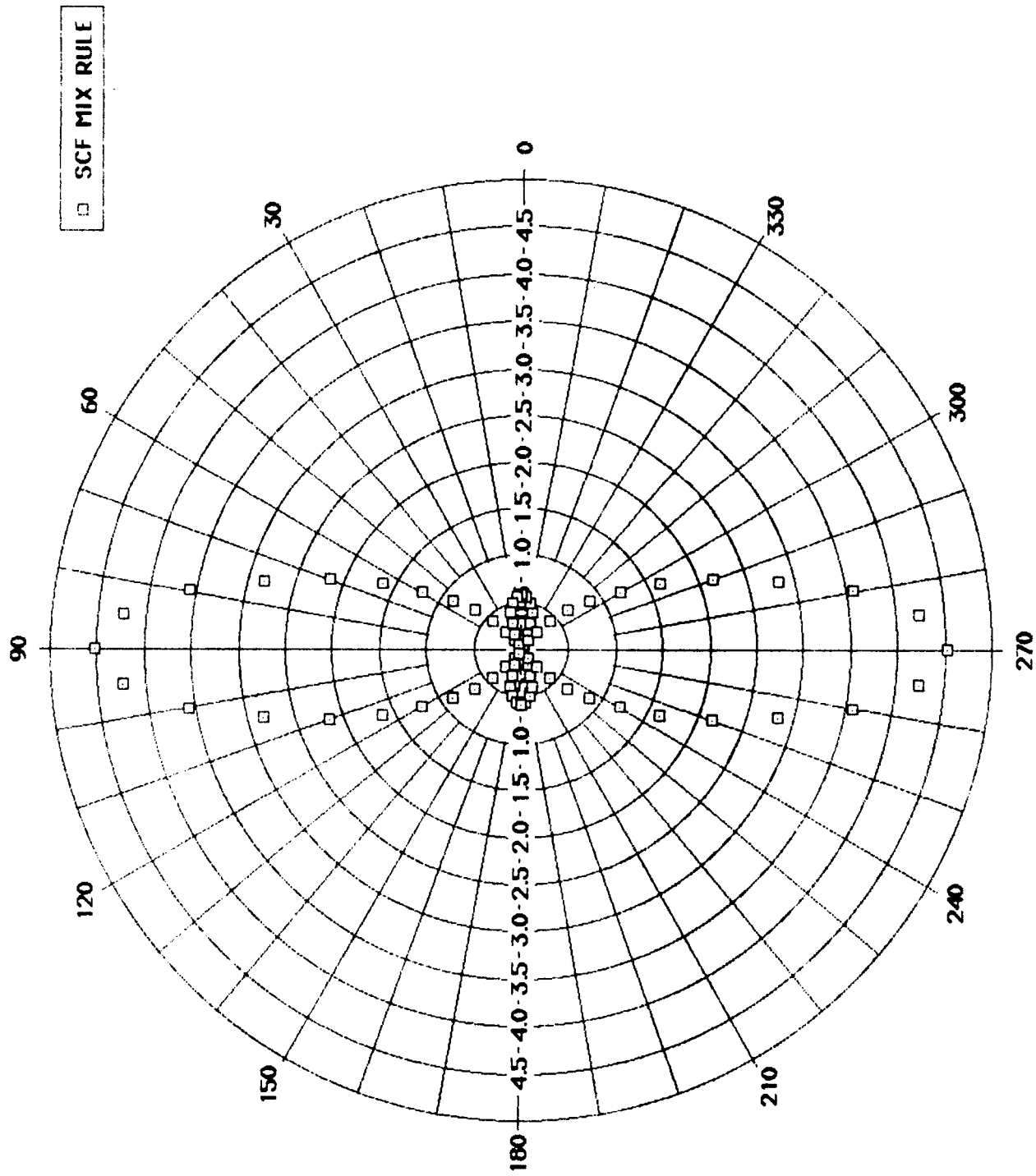
1. Ko, W.L.: *Stress Concentration Around a Small Circular Hole in the HiMAT Composite Plate*, NASA TM-86038, Dec. 1985.
2. Savin, G.N.: *Stress Distribution Around Holes*, NASA TT F-607, 1970.
3. Lekhnitskii, S.G.; Tsai, S.W.; and Cheron, T.: *Anisotropic Plates*. Gordon and Breach Science Publishers, New York, 1968.
4. Nuismer, R.J.; and Whitney, J.M.: Uniaxial failure of composite laminates containing stress concentrations. In *Fracture Mechanics of Composites*, ASTM ATP 593, 1975, pp. 117-142.
5. Whitney, J.M.; and Nuismer, R.J.: Stress fracture criteria for laminated composite containing stress concentration. *J. Comp. Materials*, vol. 8, pp. 253-265, 1974.
6. Yeh, H.Y.: *Stress Concentration Around Circular Hole in a Composite Material Specimen Representative of the X-29A Forward-Swept Wing Aircraft*. NASA CR-179435, Aug. 1988.
7. Calote, L.R.: *The Analysis of Laminated Composite Structures*. Van Nostrand Reinhold Co., New York, 1969.
8. Jones, R.M.: *The Mechanics of Composite Materials*. McGraw-Hill Book Co., New York, 1975.
9. Tsai, S.W.; and Hahn, H.T.: *Introduction to Composite Materials*. Technomic Publishing Company, Inc., 1980.



ALPHA (DEG)
 Figure 1. SCF correlation for $\phi = 0^\circ$, -60°F .



270
 Figure 2. SCF for $\phi = 0^\circ$, -60°F .



270
Figure 3. SCF for $\phi = 0^\circ, -60^\circ\text{F}$.

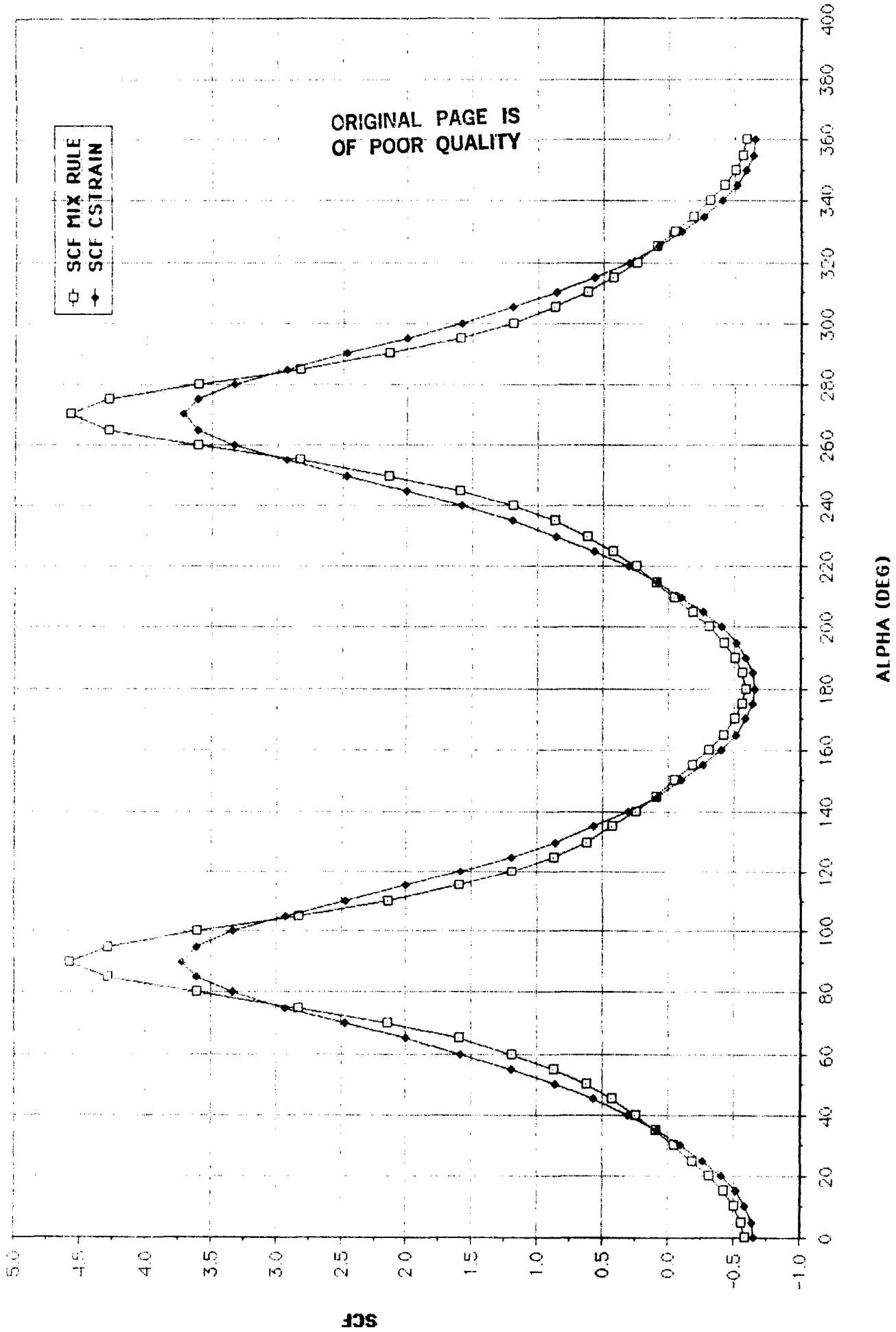


Figure 4. SCF correlation for $\phi = 0^\circ, 70^\circ\text{F}$.

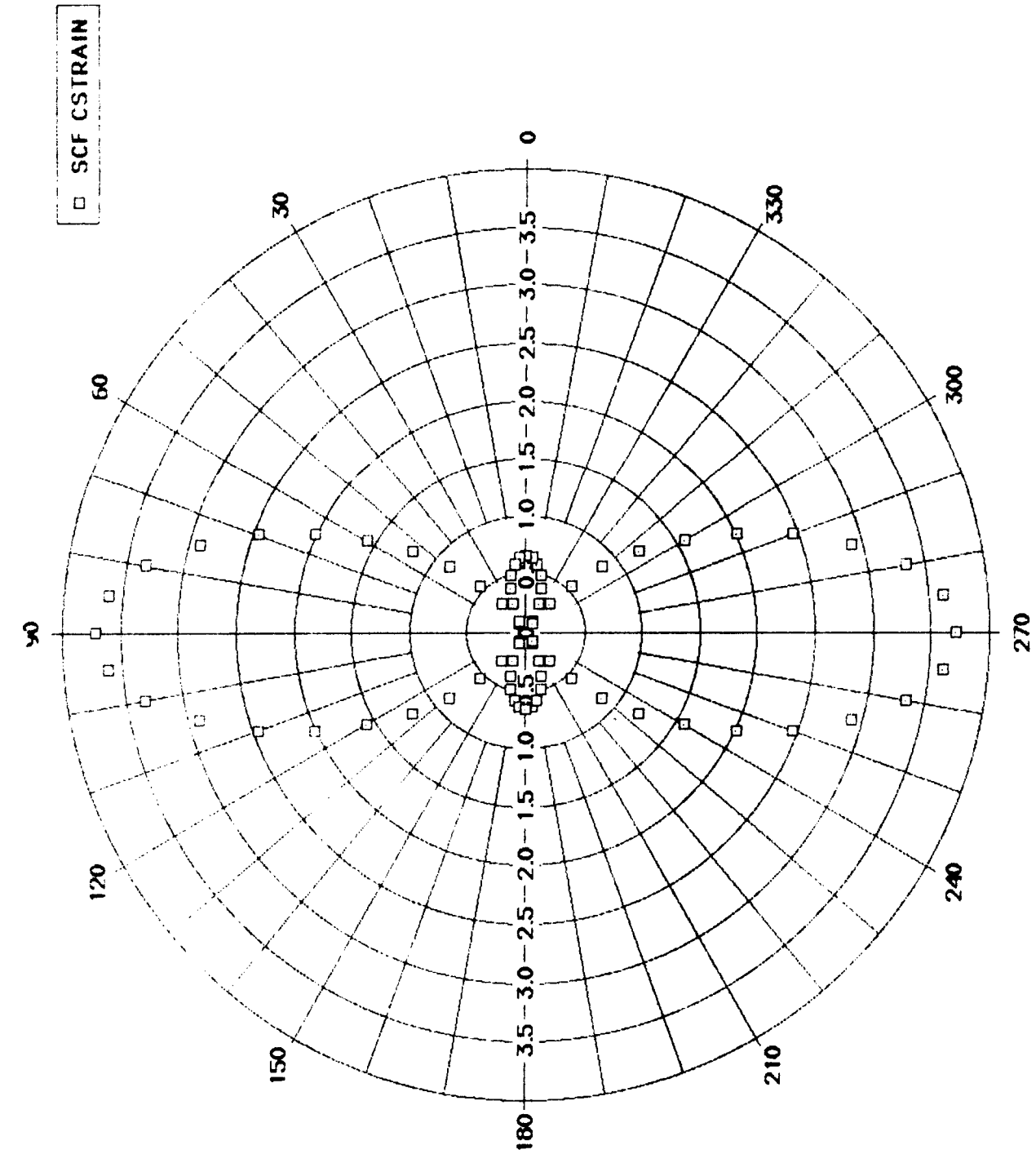
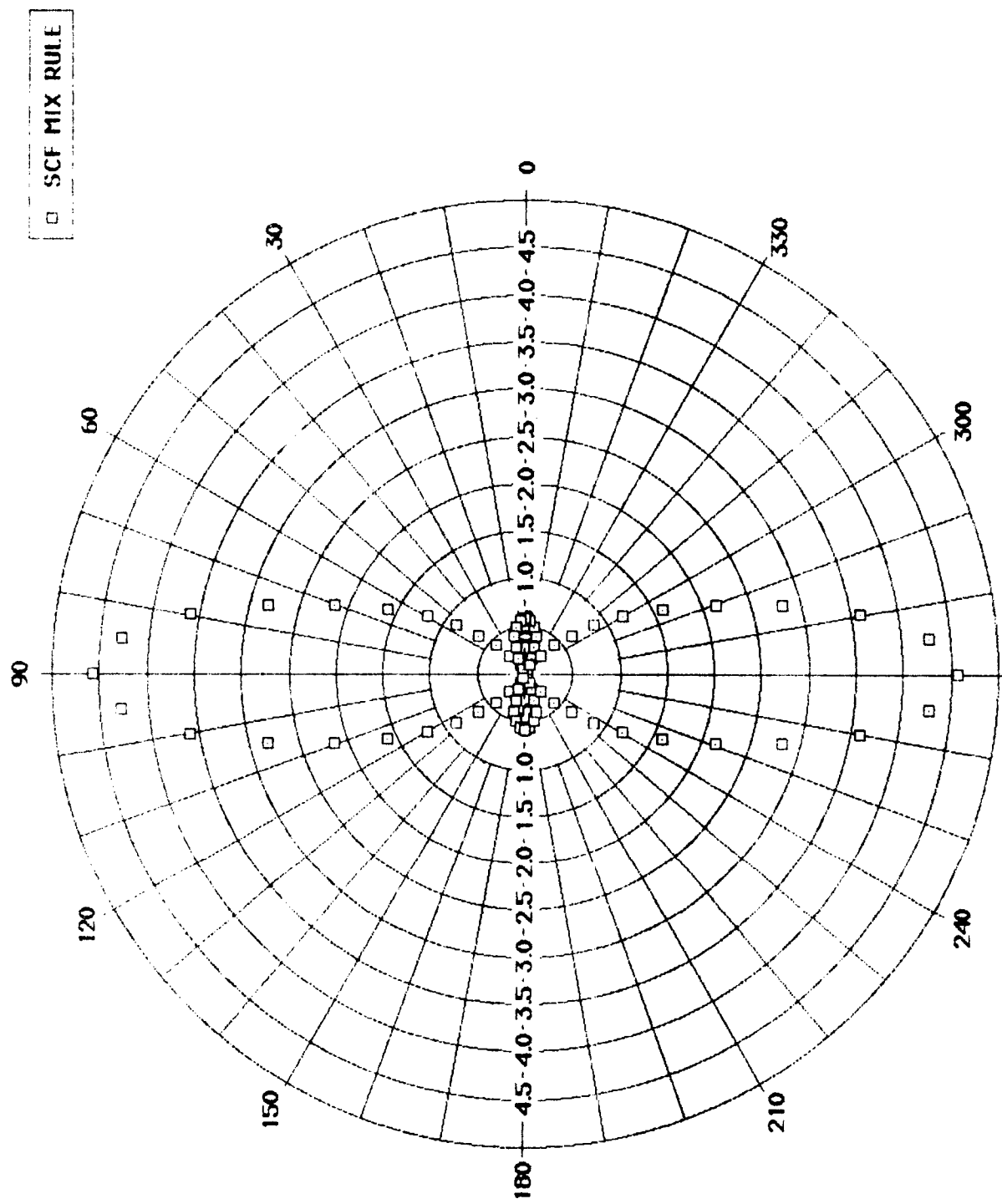
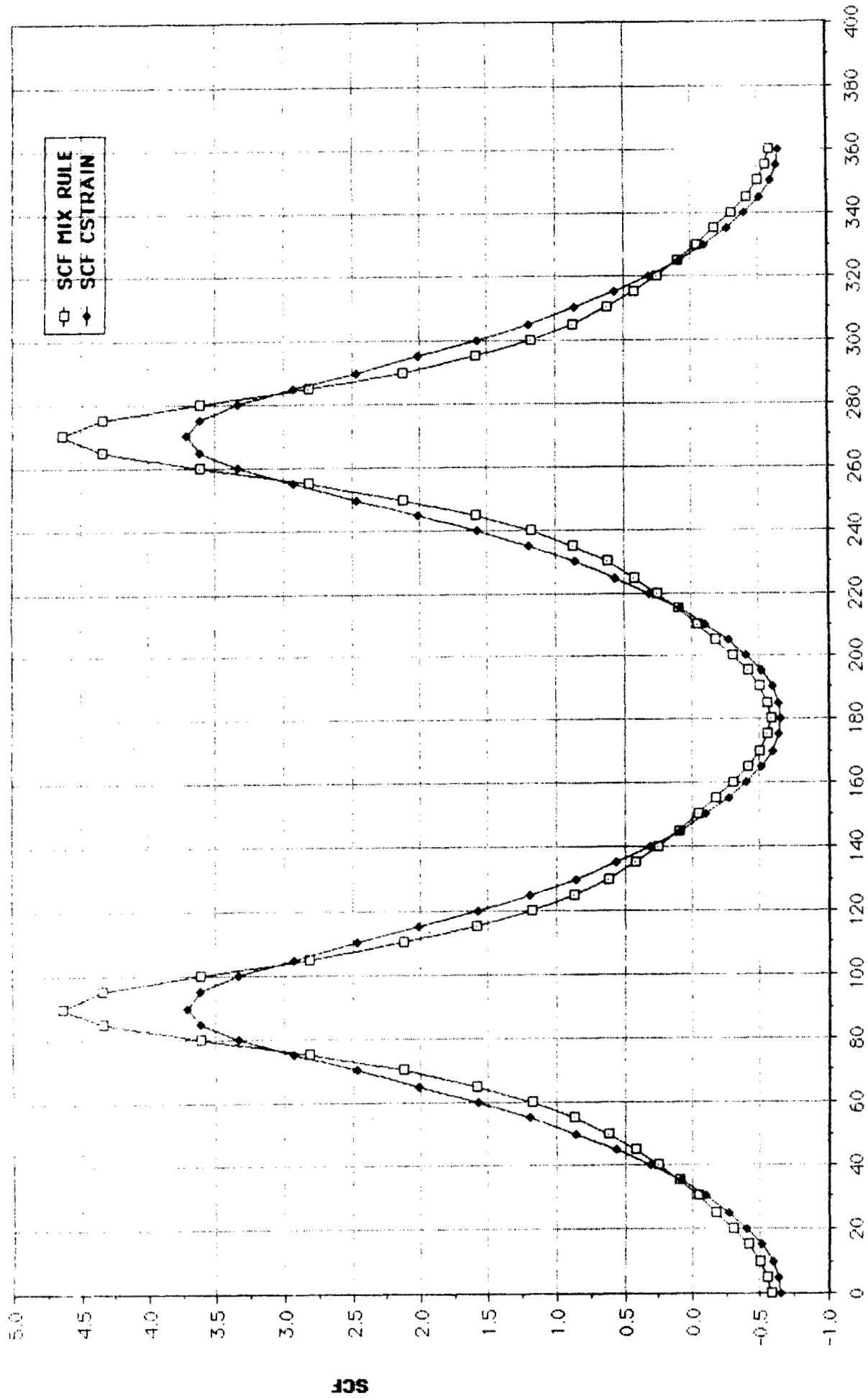


Figure 5. SCF for $\phi = 0^\circ$, 70°F .



270
 Figure 6. SCF for $\phi = 0^\circ$, 70°F .



ALPHA (DEG)
 Figure 7. SCF correlation for $\phi = 0^\circ$, 200°F .

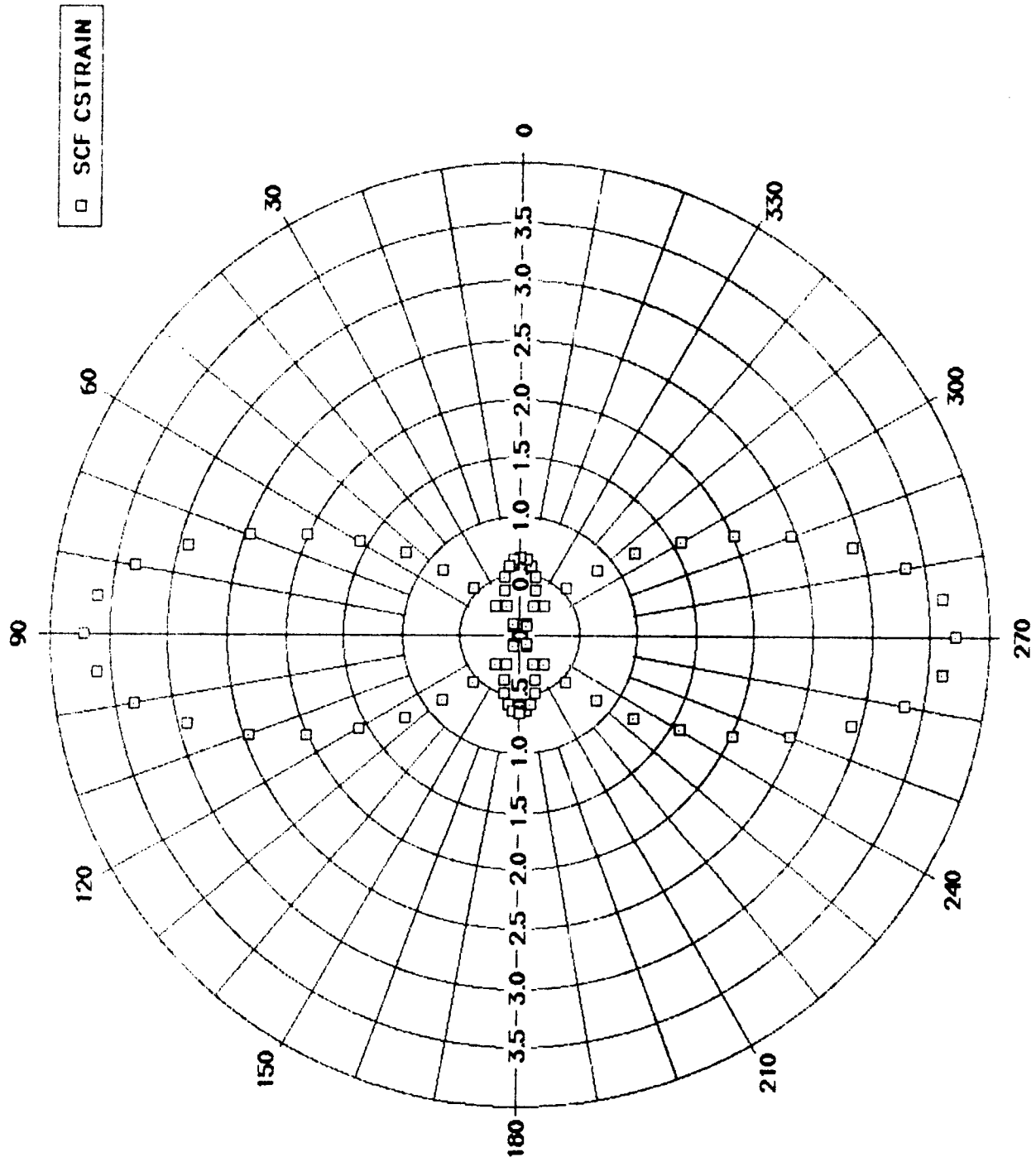


Figure 8. SCF for $\phi = 0^\circ$, 200°F .

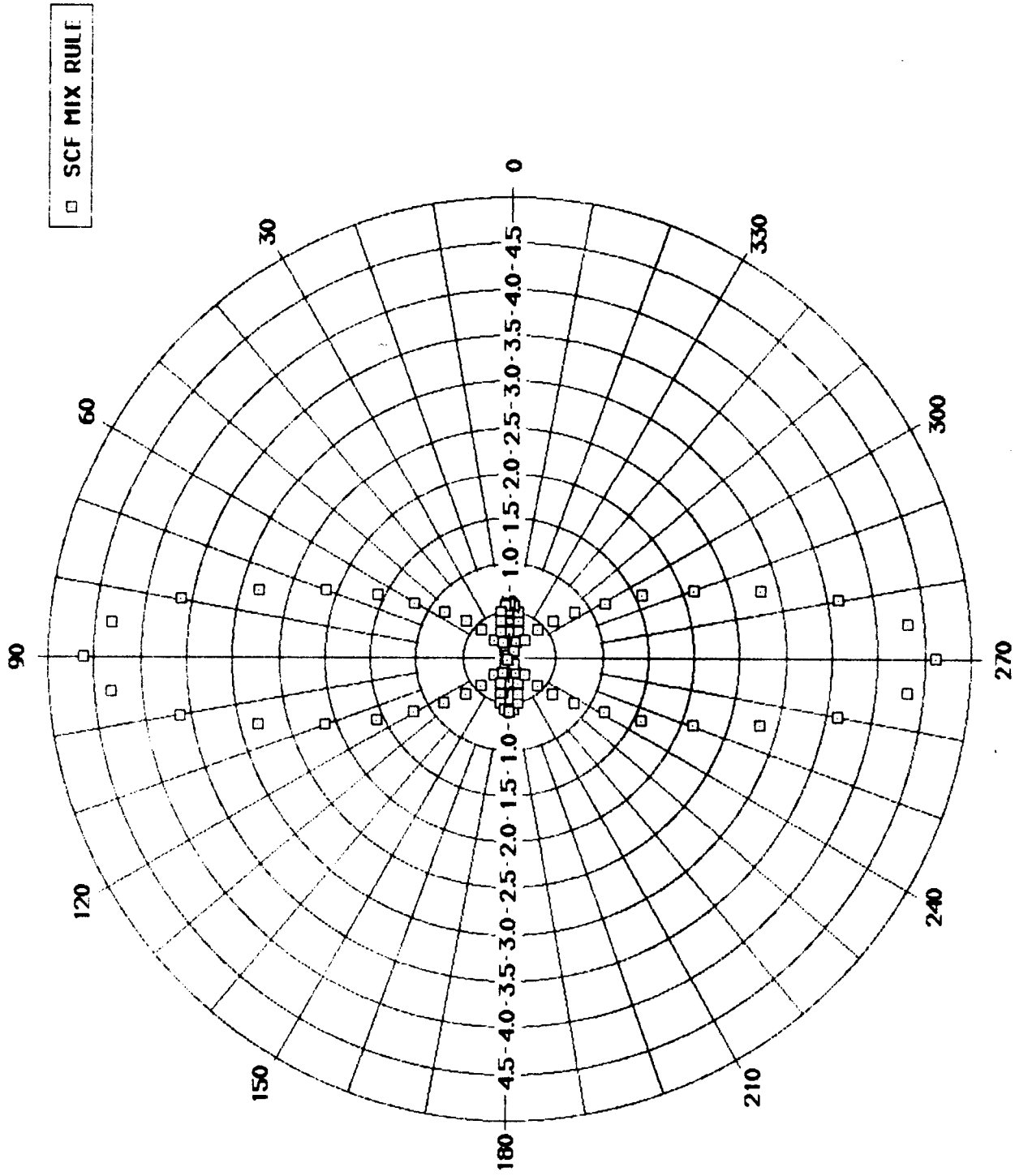
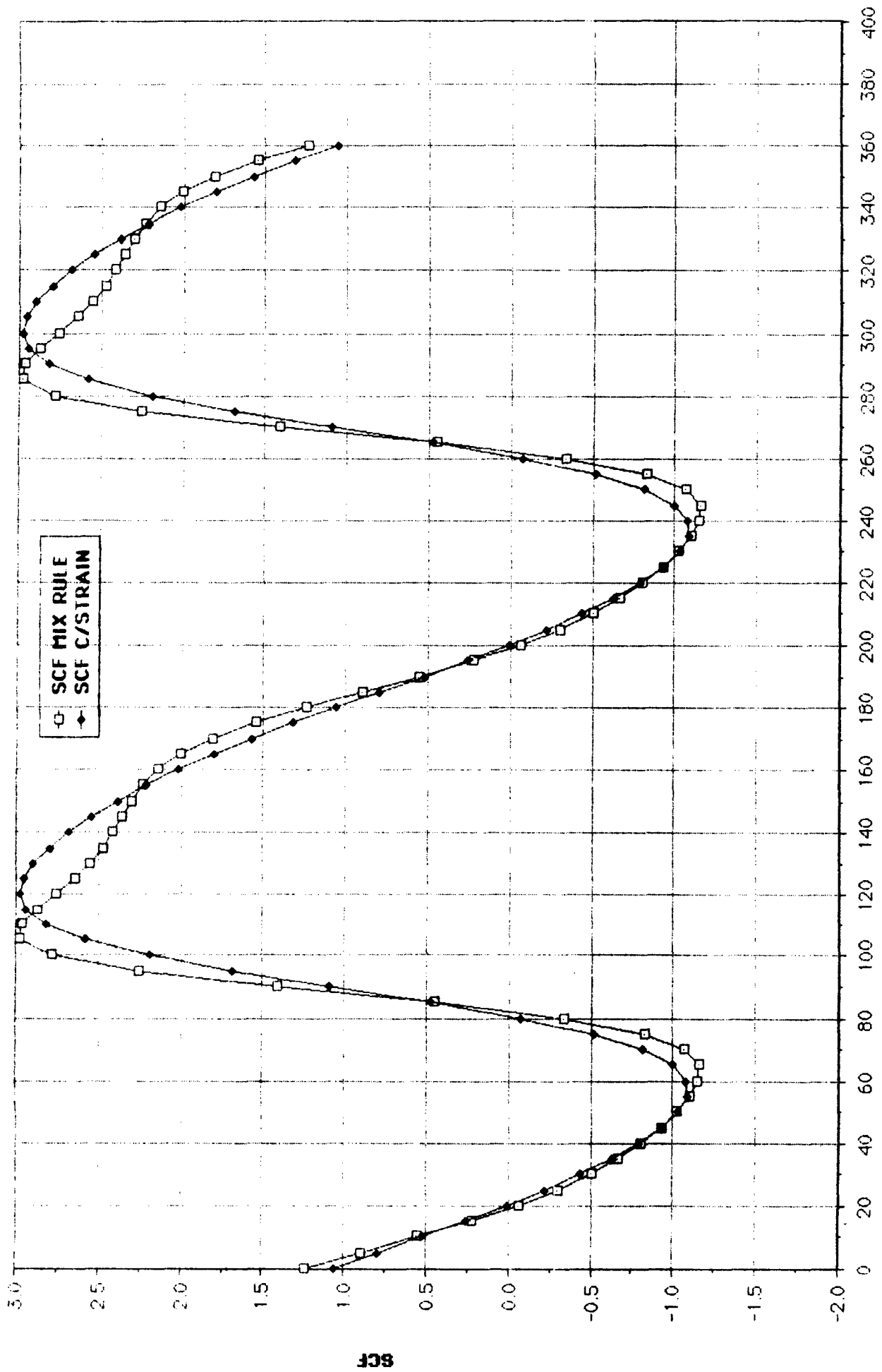


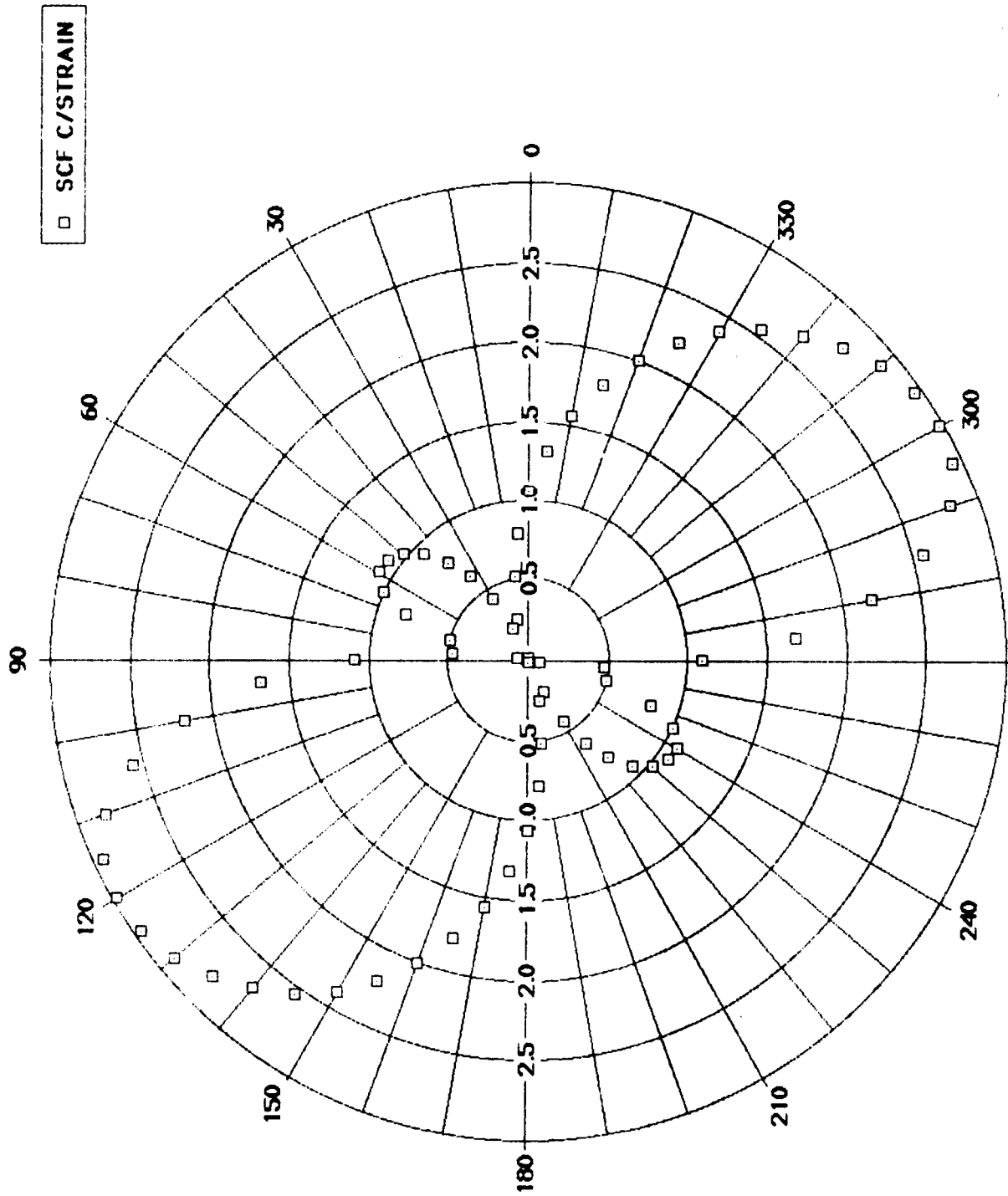
Figure 9. SCF for $\phi = 0^\circ$, 200°F .

270



ALPHA (DEG)

Figure 10. SCF correlation for $\phi = 45^\circ$, -60°F .



270

Figure 11. SCF for $\phi = 45^\circ$, -60°F .

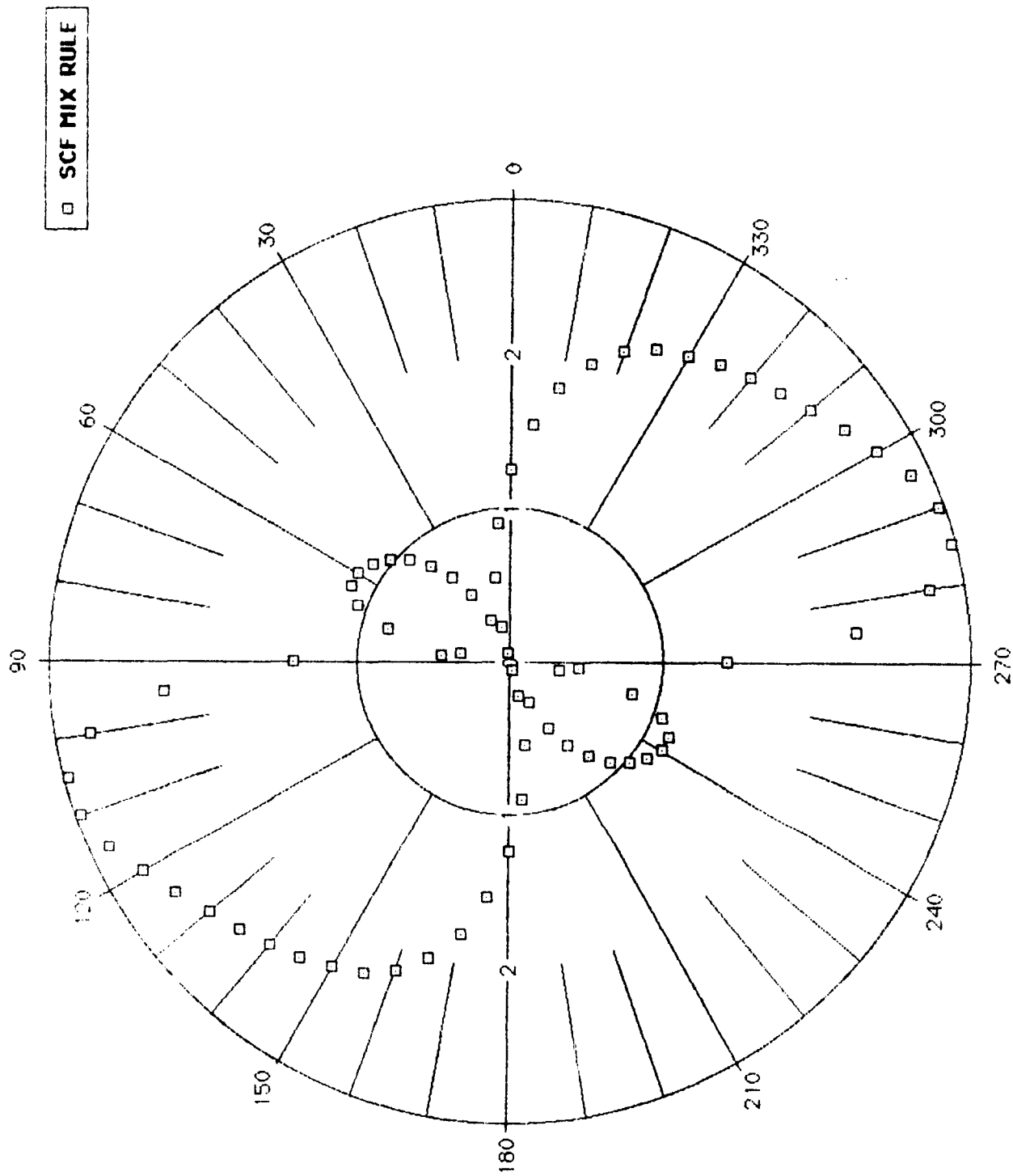
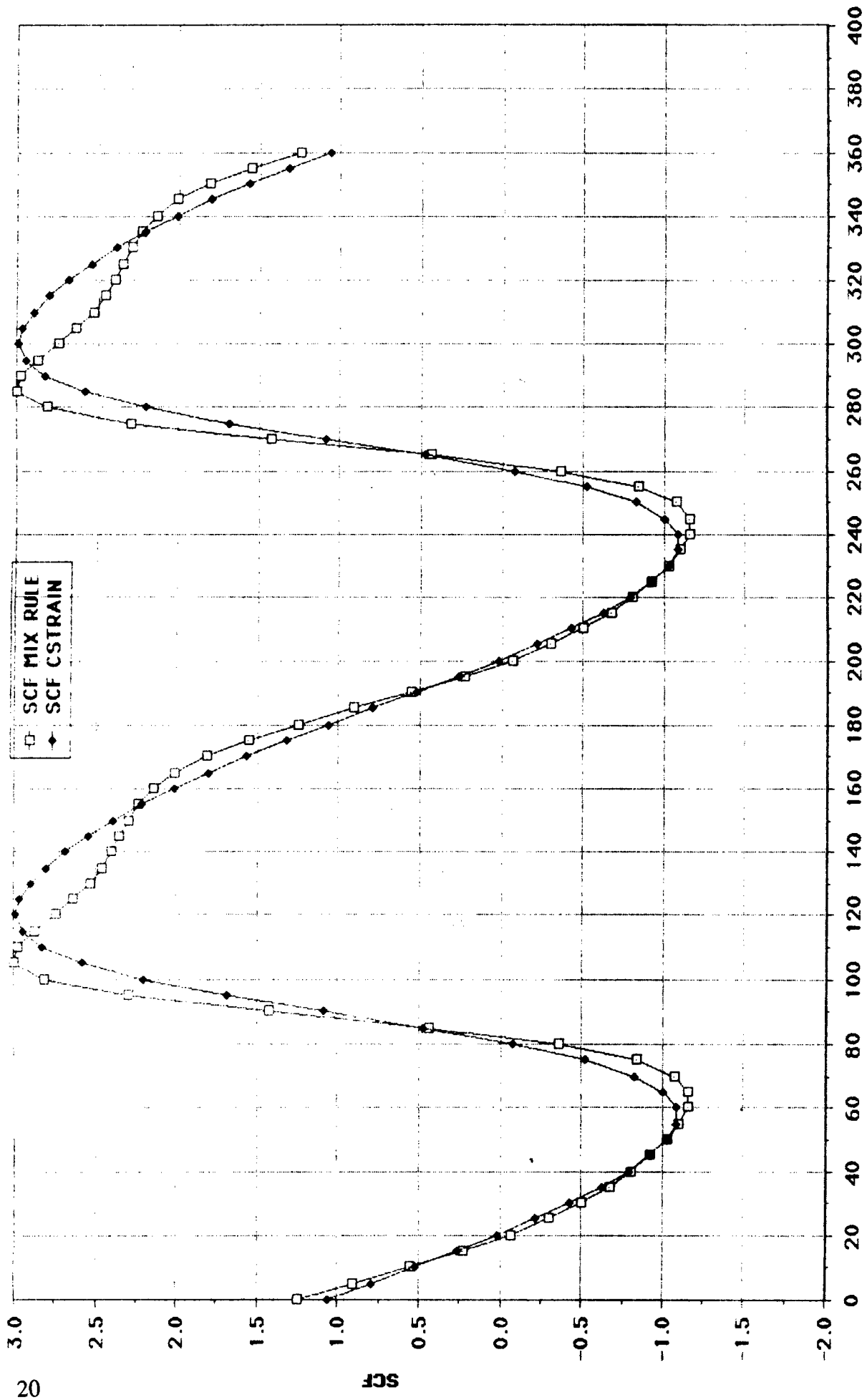
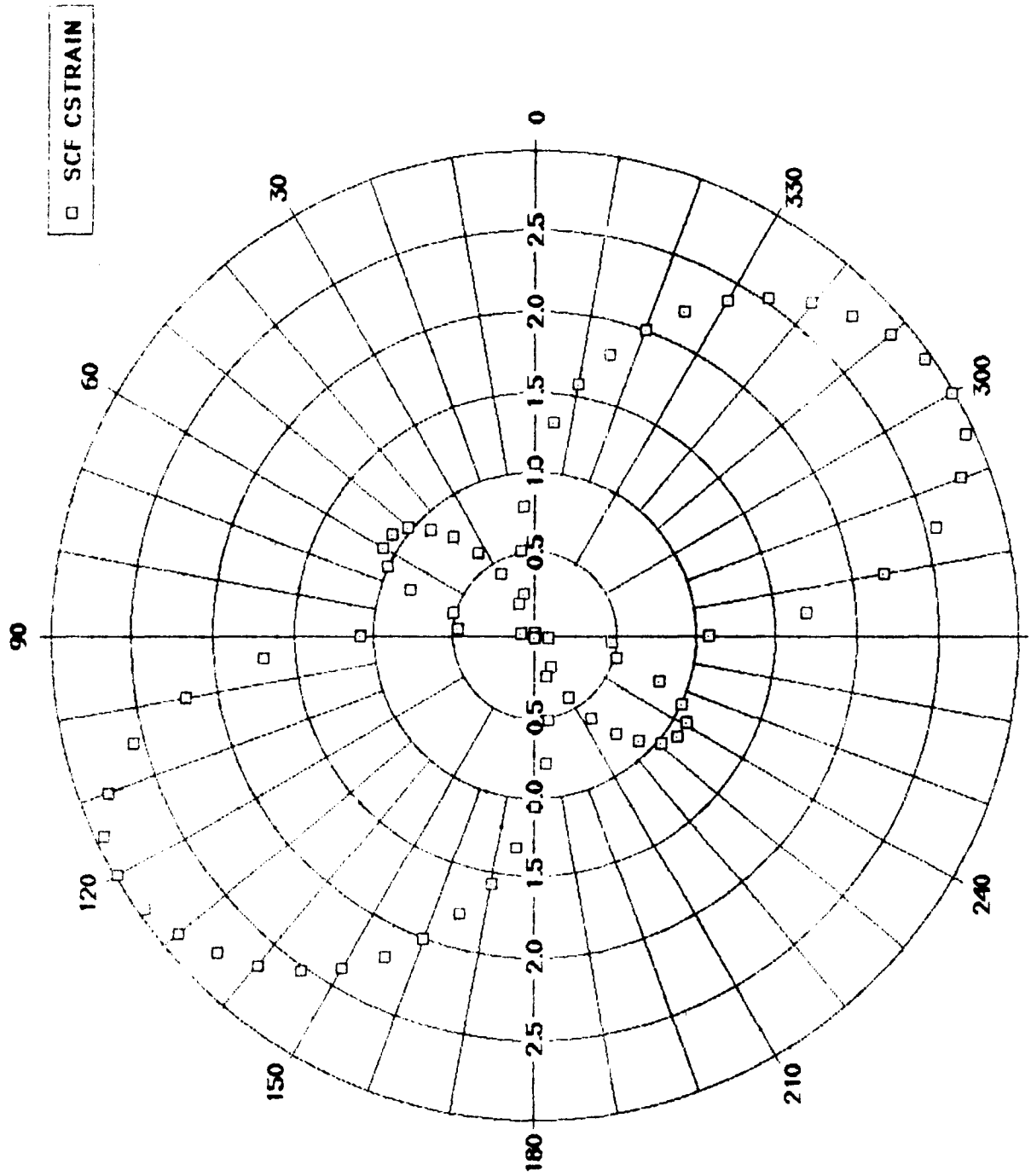


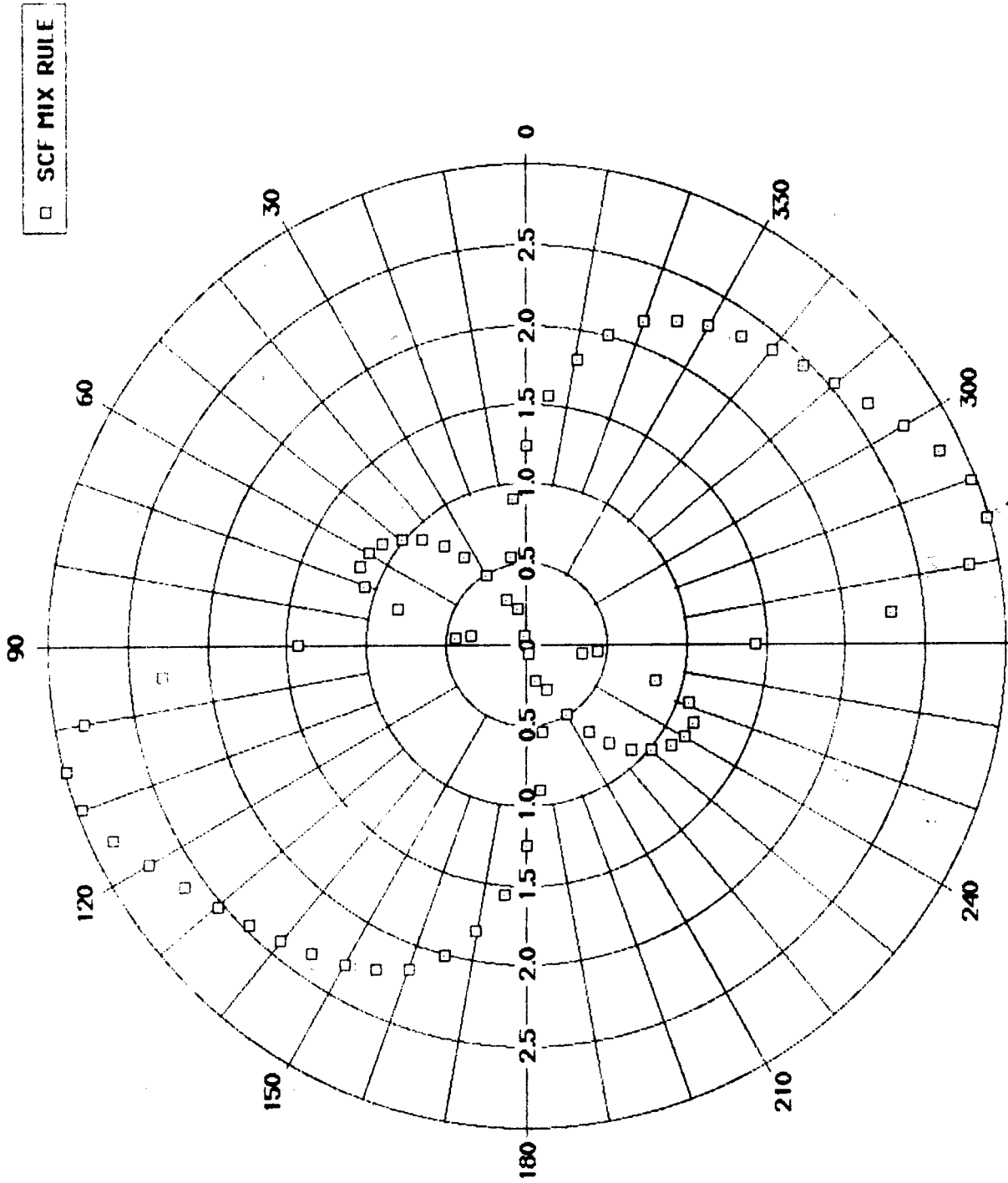
Figure 12. SCF for $\phi = 45^\circ$, -60°F .



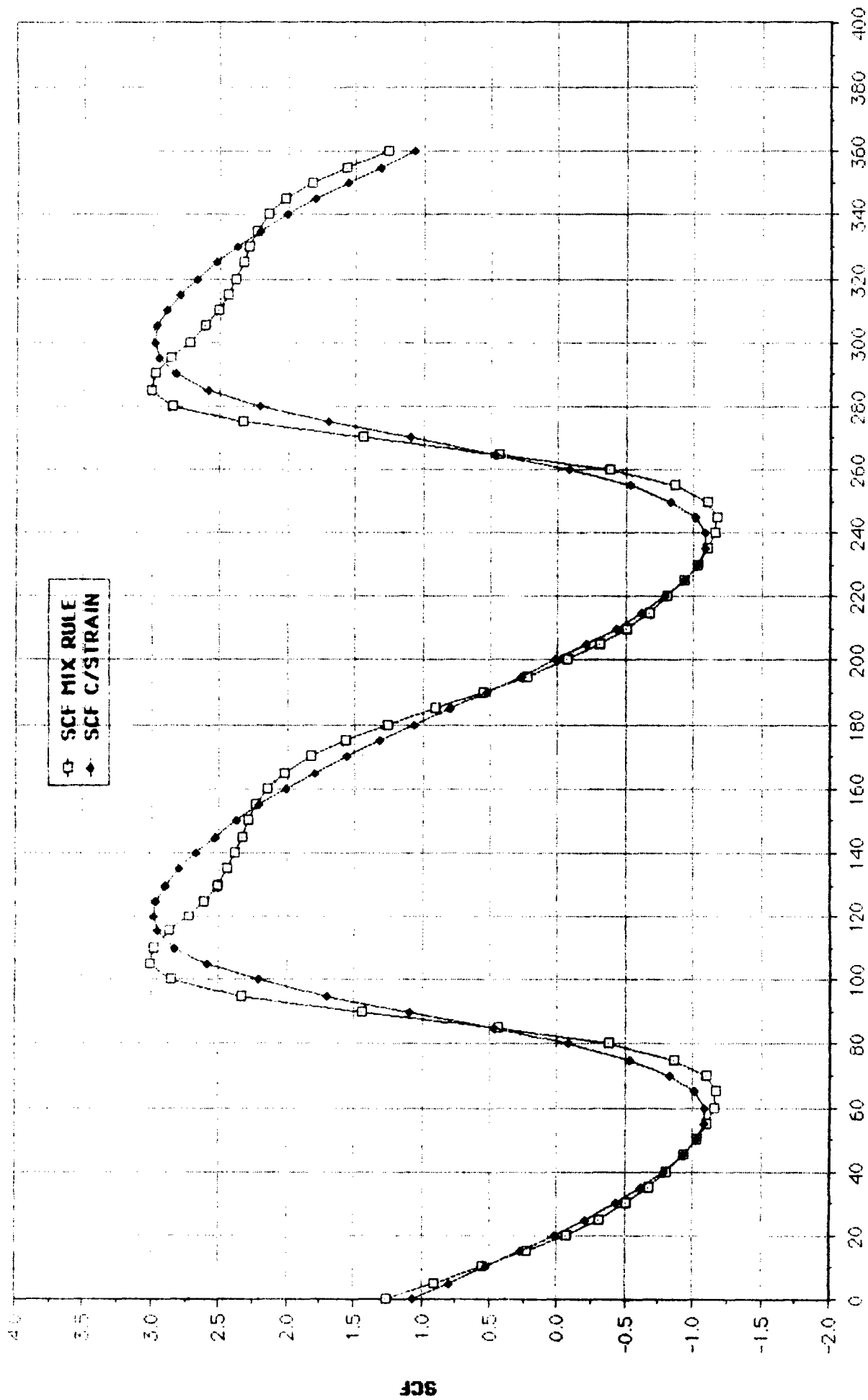
ALPHA (DEG)
 Figure 13. SCF correlation for $\phi = 45^\circ$, 70°F .



270
 Figure 14. SCF for $\phi = 45^\circ, 70^\circ\text{F}$.

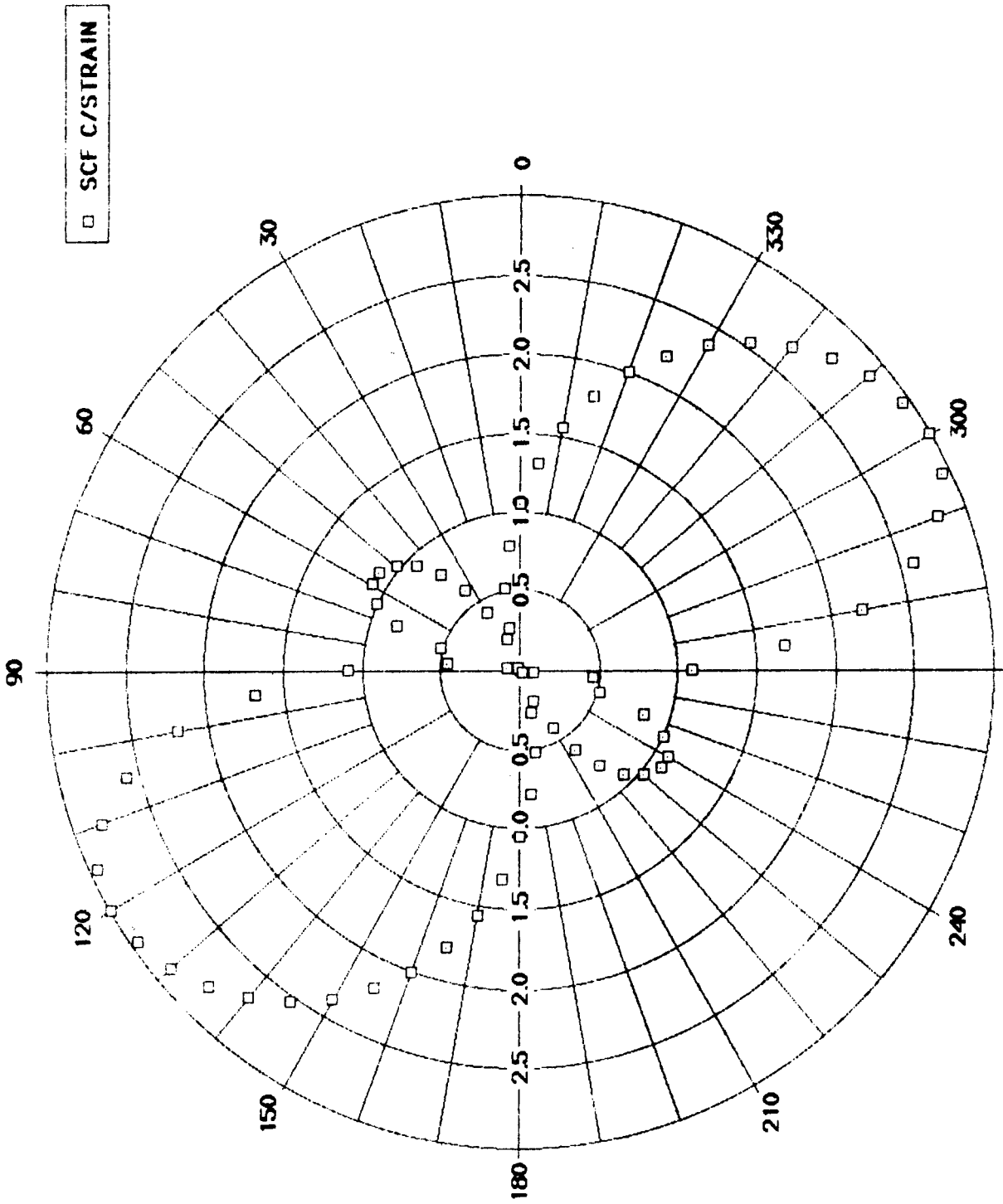


270
Figure 15. SCF for $\phi = 45^\circ, 70^\circ\text{F}$.

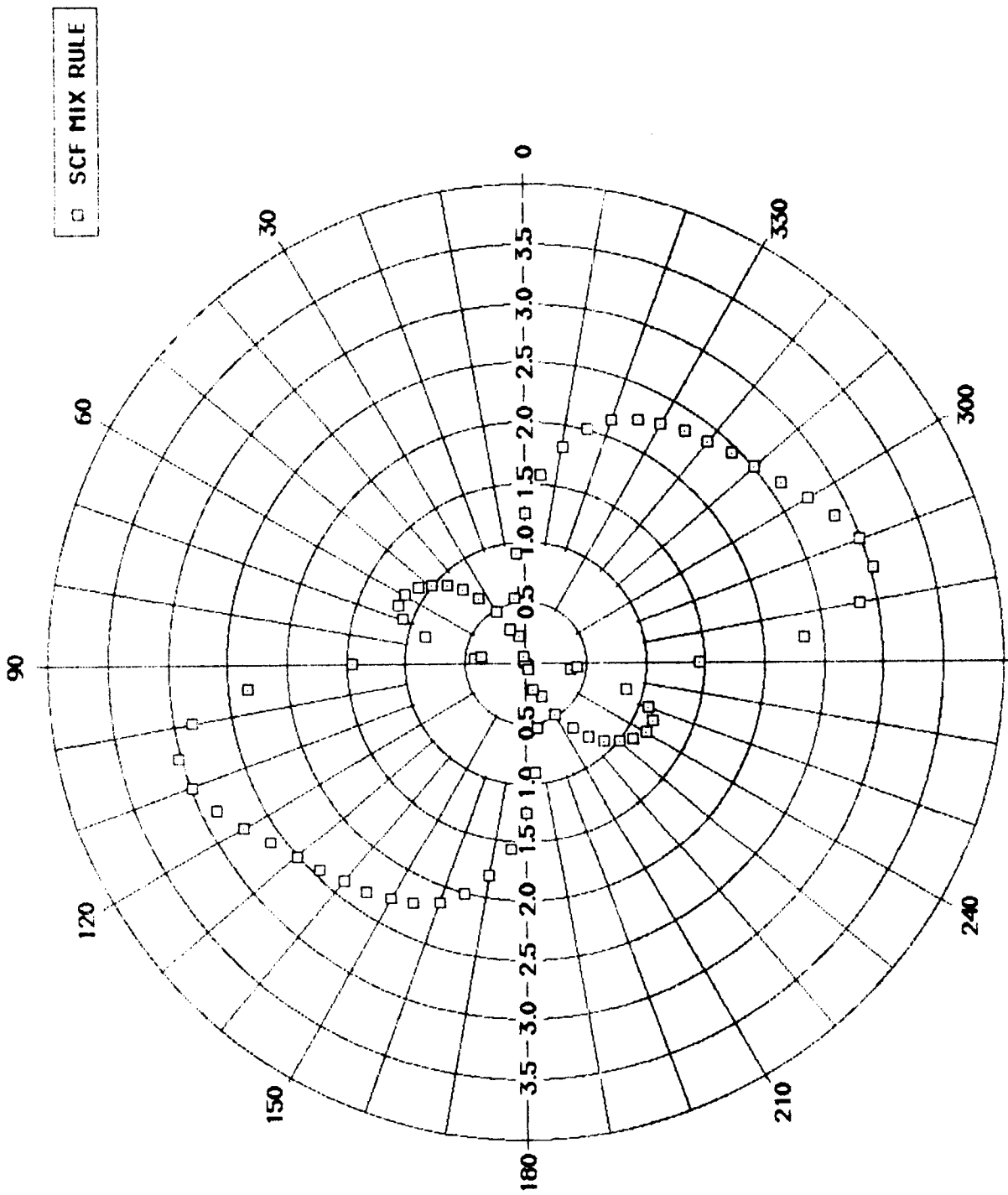


ALPHA (DEG)

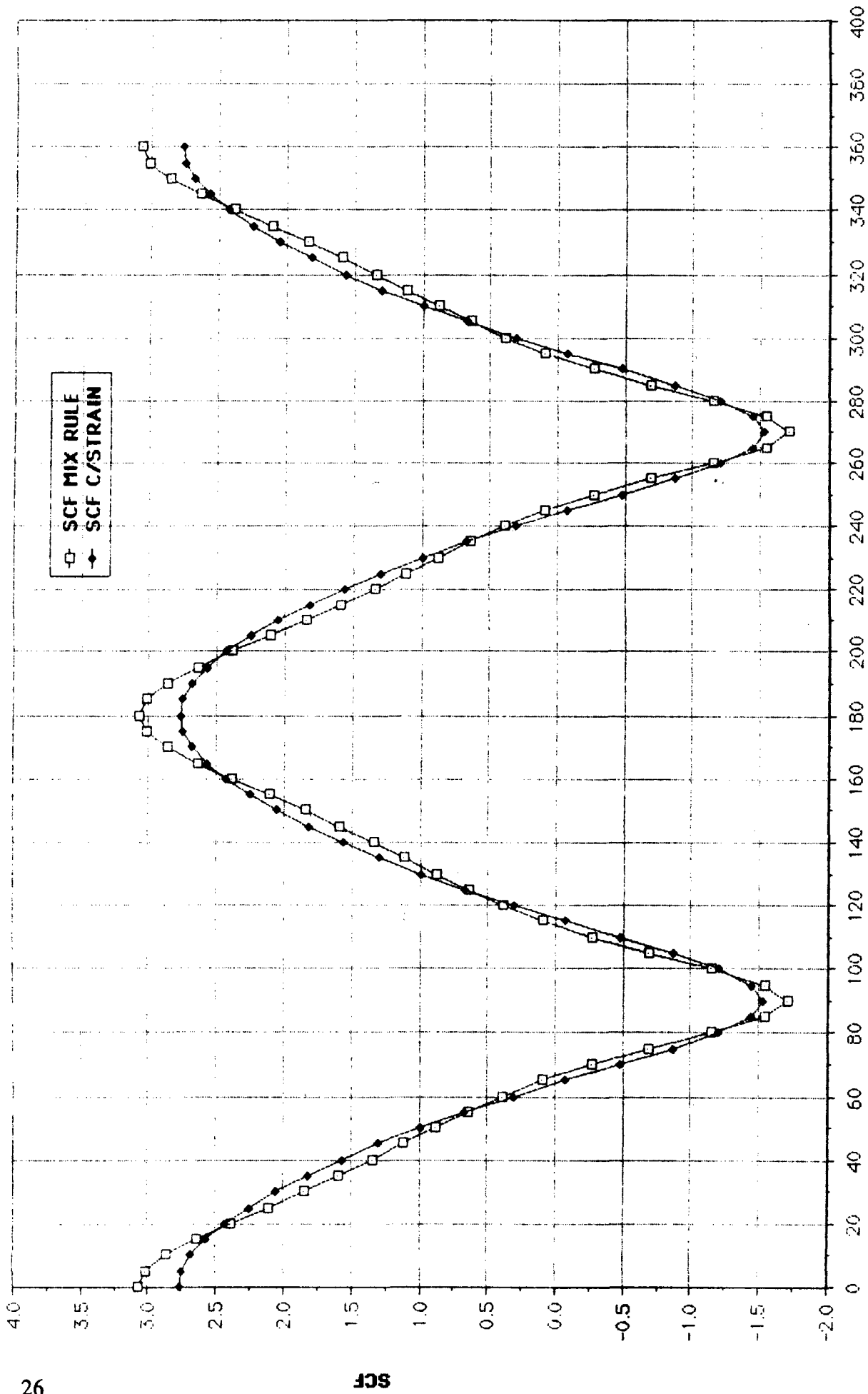
Figure 16. SCF correlation for $\phi = 45^\circ, 200^\circ\text{F}$.



270
 Figure 17. SCF for $\phi = 45^\circ, 200^\circ\text{F}.$



270
 Figure 18. SCF for $\phi = 45^\circ$, 200°F .



ALPHA (DEG)

Figure 19. SCF correlation for $\phi = 90^\circ - 60^\circ\text{F}$.

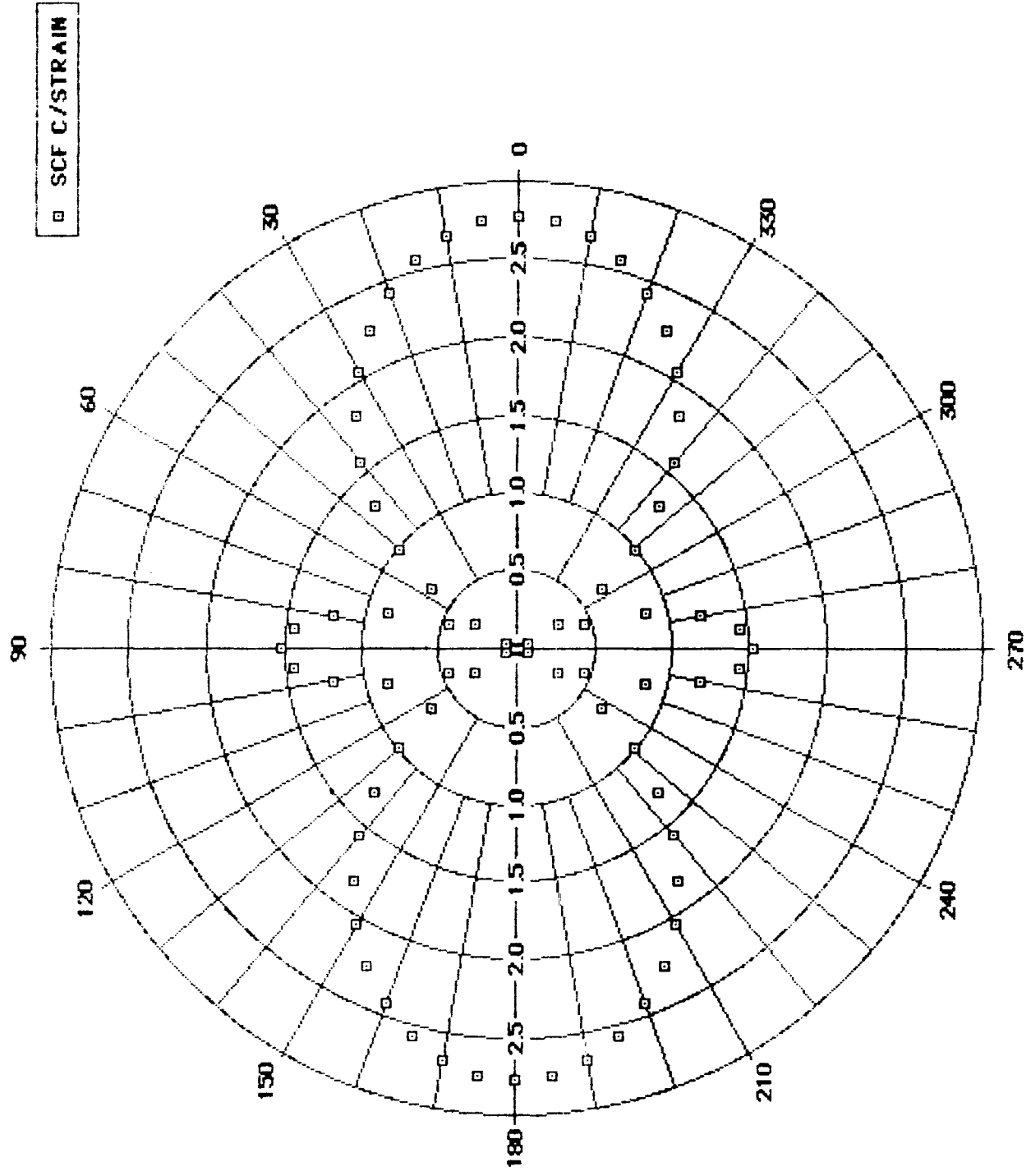


Figure 20. SCF for $\phi = 90^\circ$, -60°F .

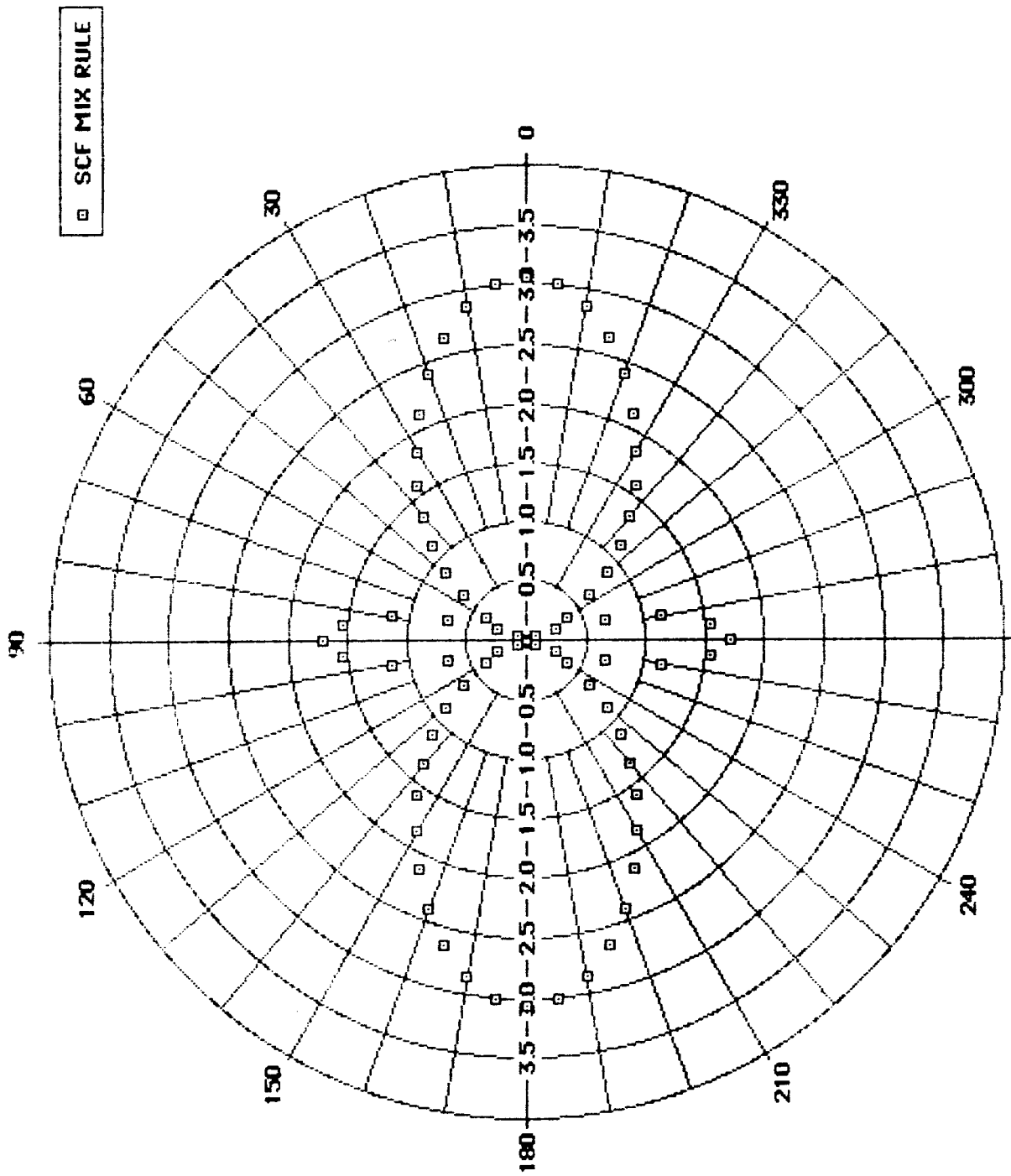


Figure 21. SCF for $\phi = 90^\circ$, 60°F .

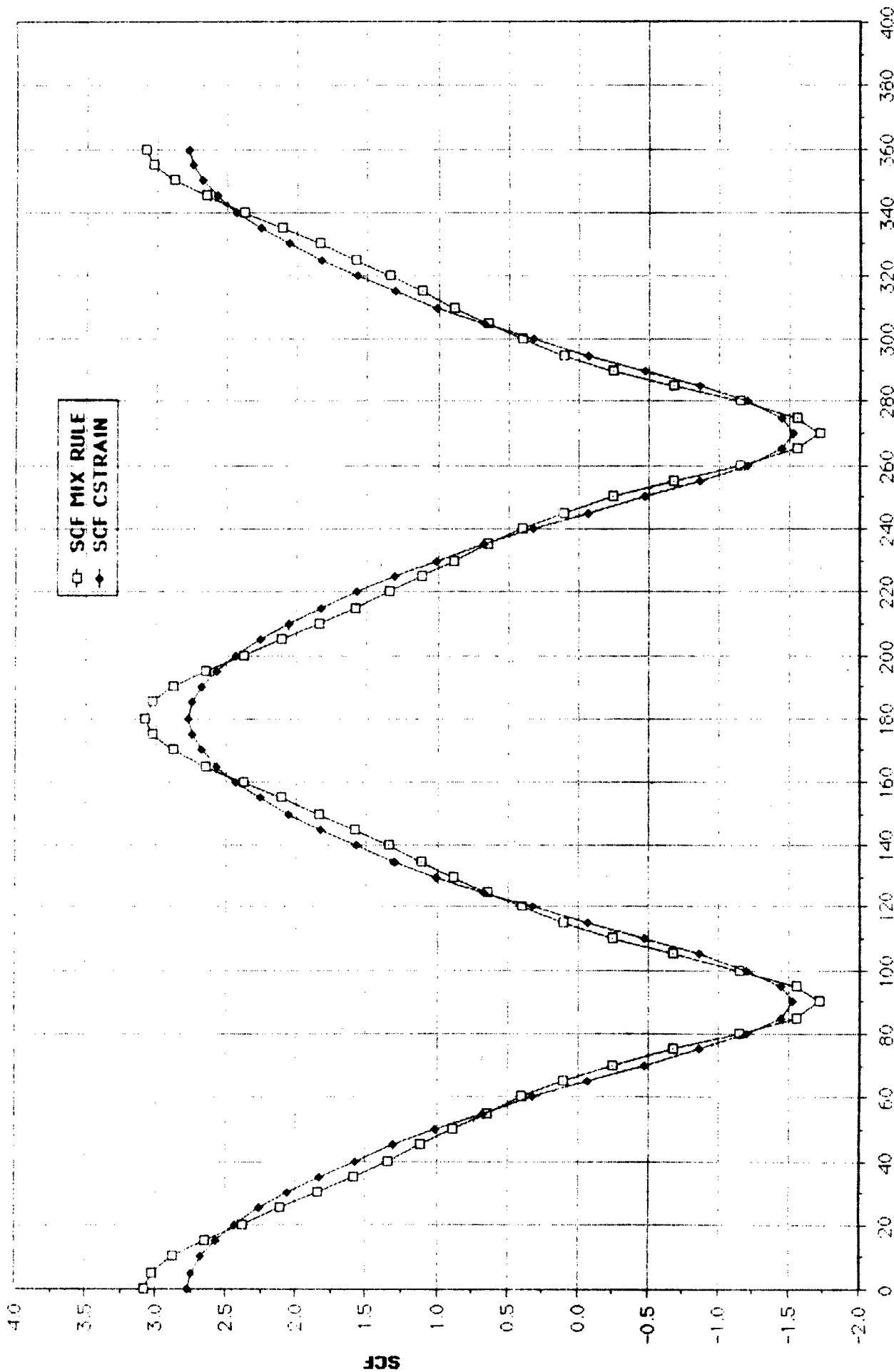
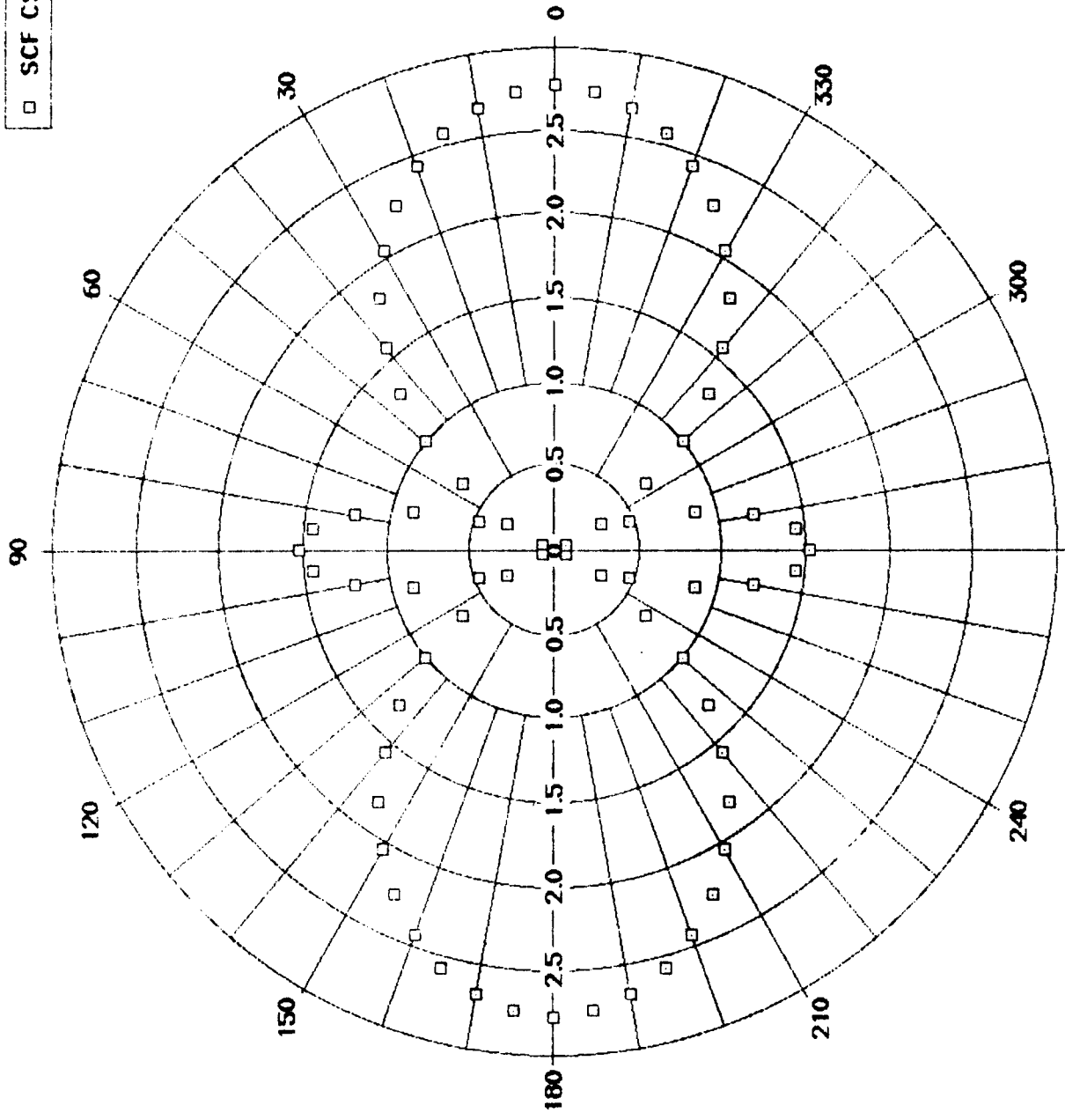


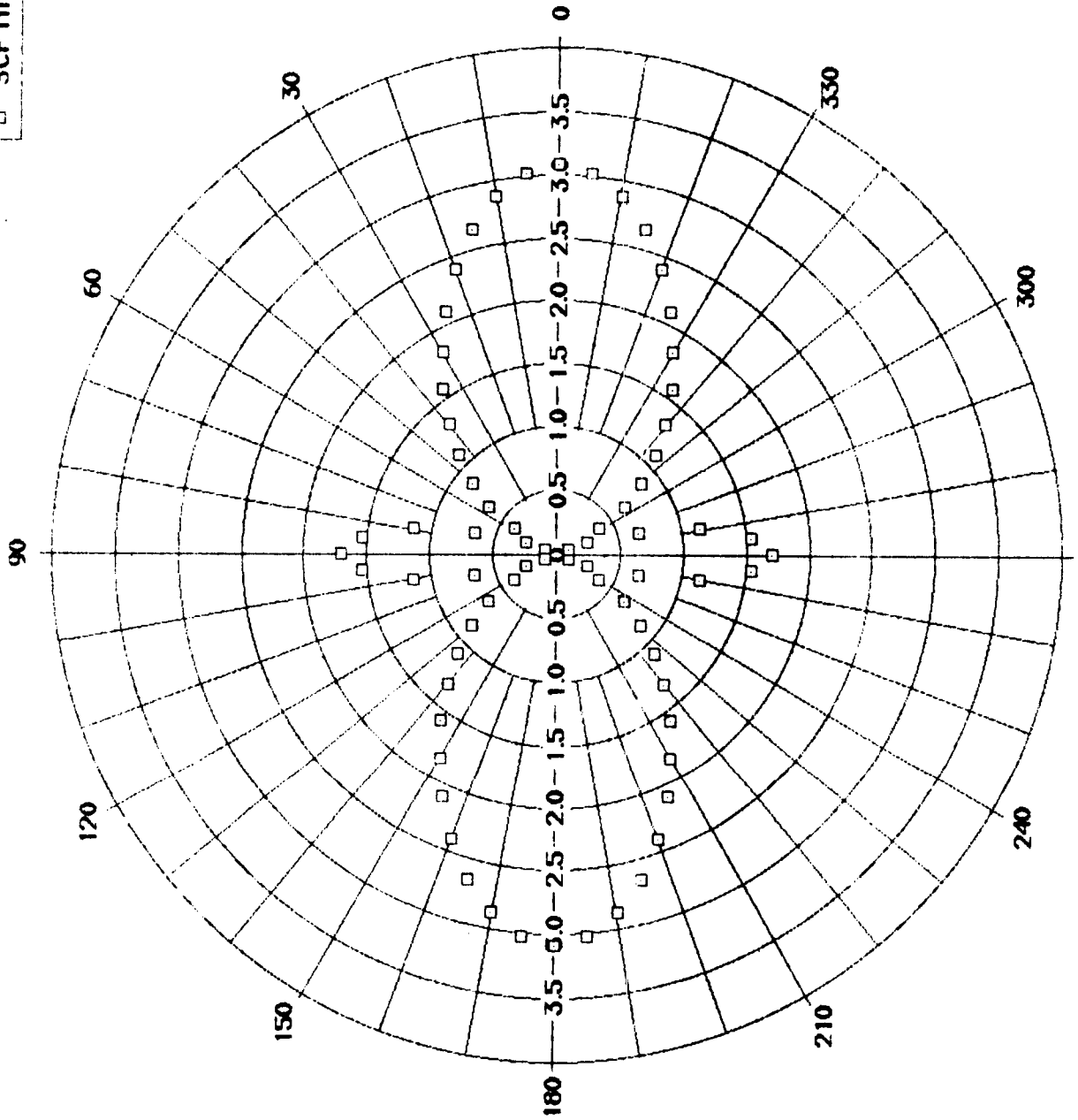
Figure 22. SCF correlation for $\phi = 90^\circ$, 70°F .

□ SCF CSTRAIN

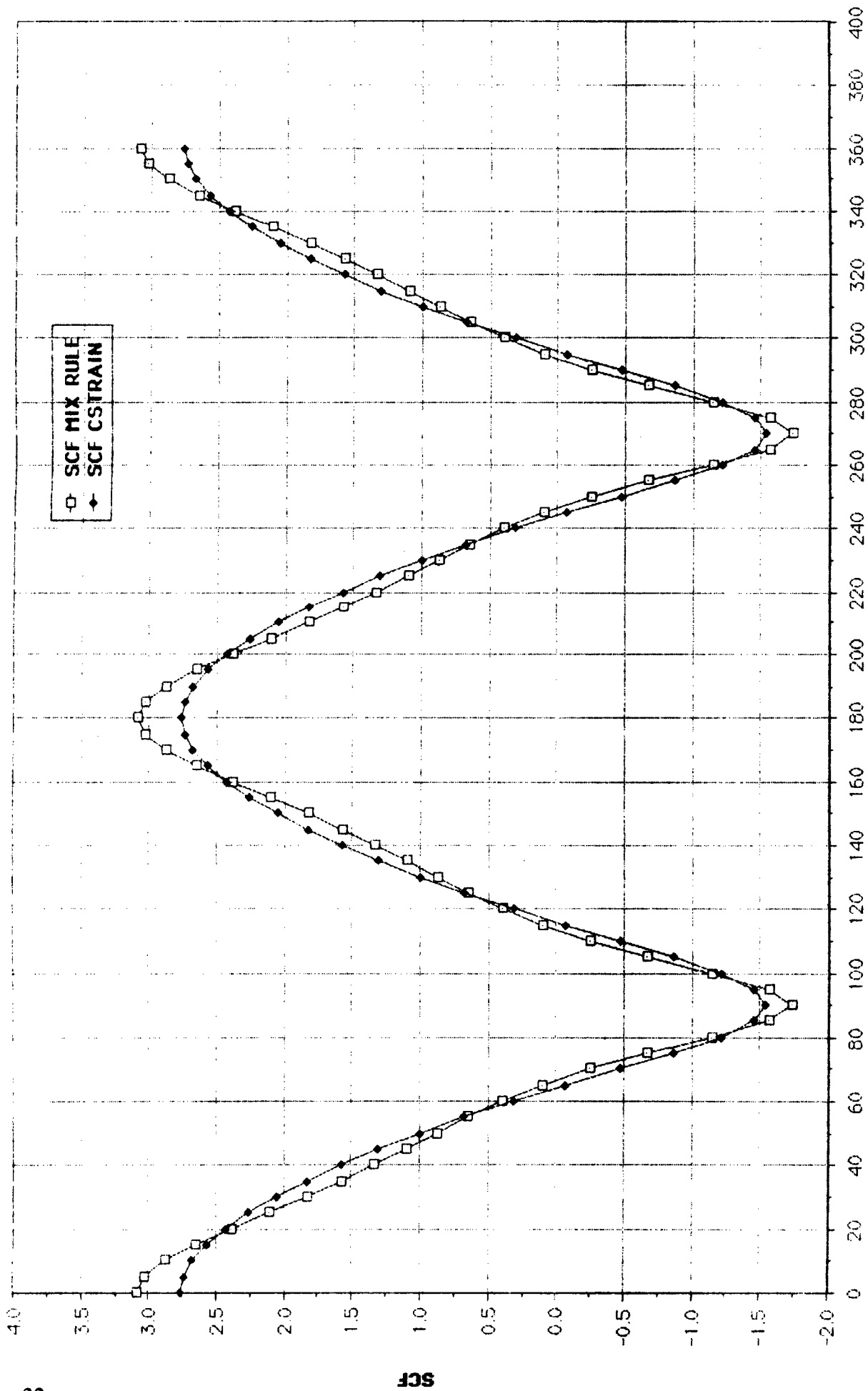


270
Figure 23. SCF for $\phi = 90^\circ, 70^\circ\text{F}$.

□ SCF MIX RULE



270
Figure 24. SCF for $\phi = 90^\circ, 70^\circ\text{F}$.



ALPHA (DEG)
 Figure 25. SCF correlation for $\phi = 90^\circ$, 200°F .

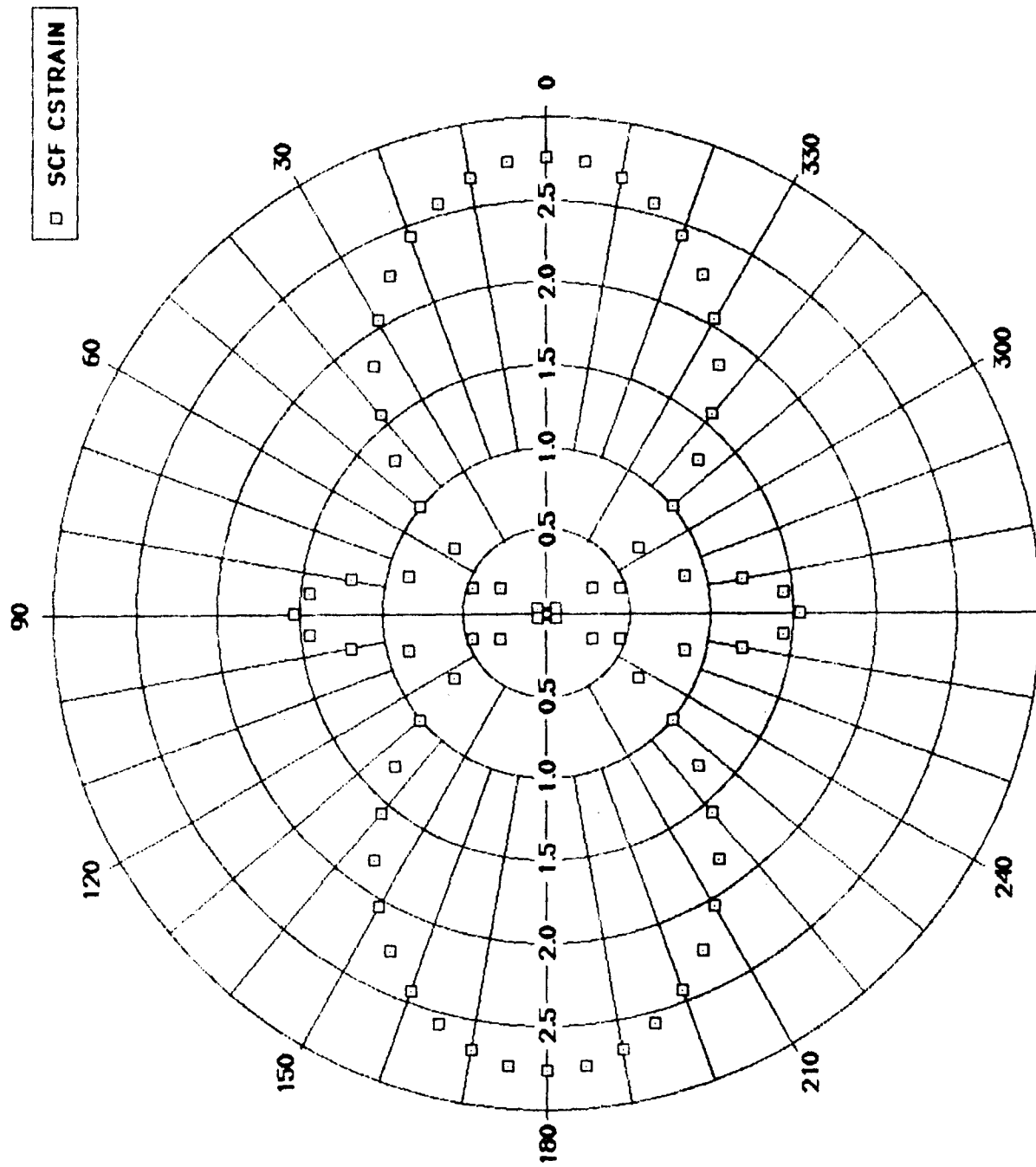
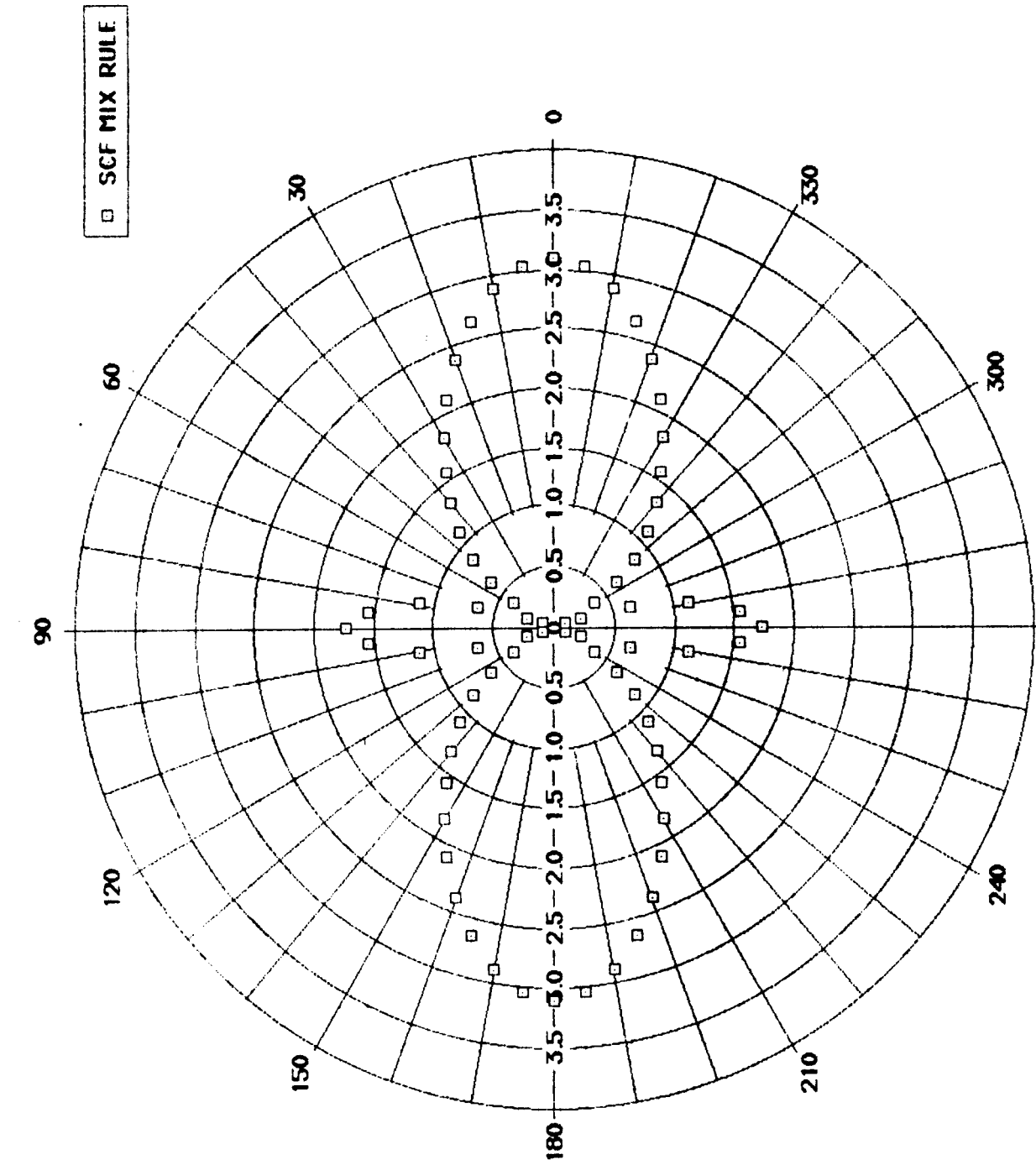


Figure 26. SCF for $\phi = 90^\circ$, 200°F.



270
 Figure 27. SCF for $\phi = 90^\circ$, 200°F .

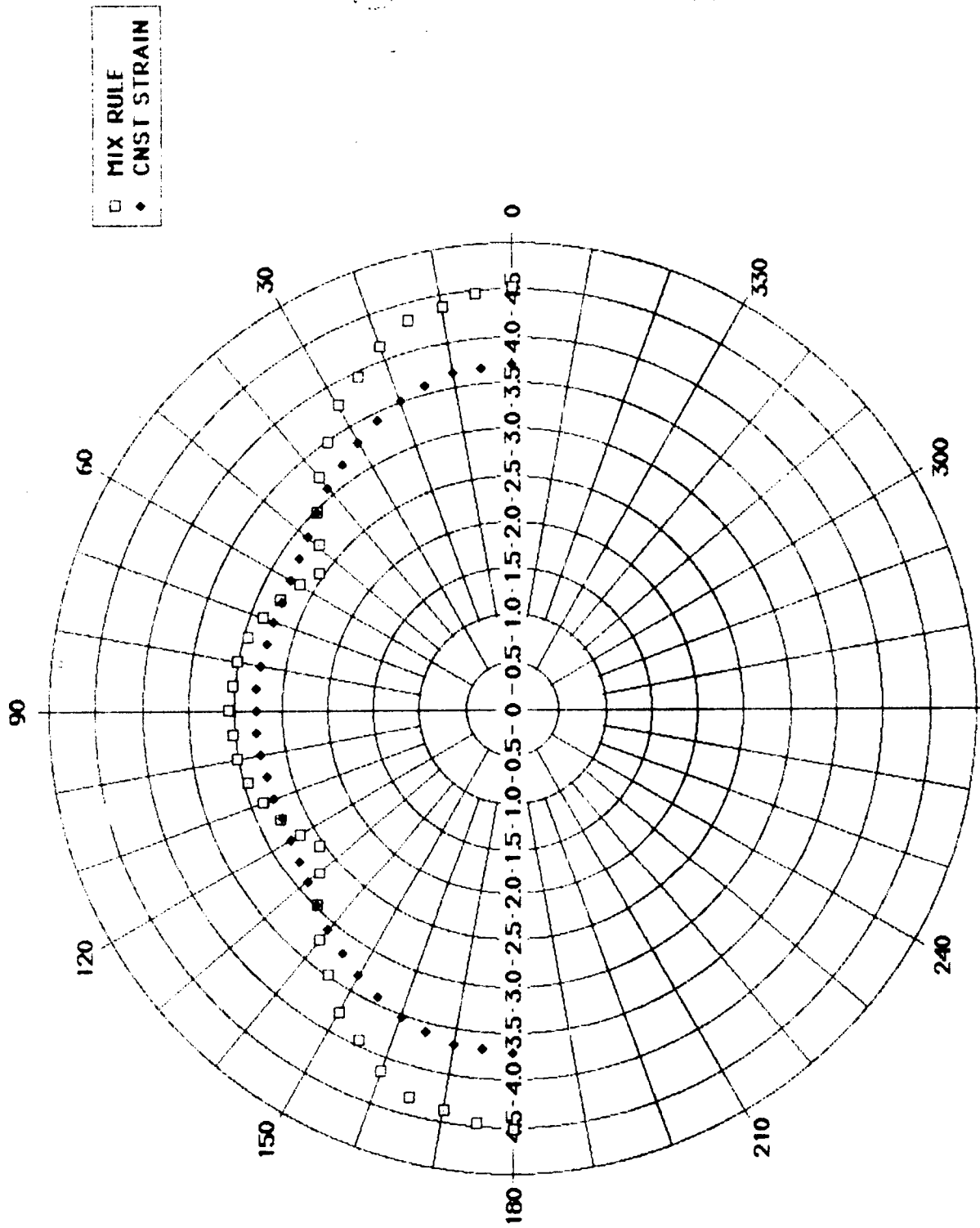
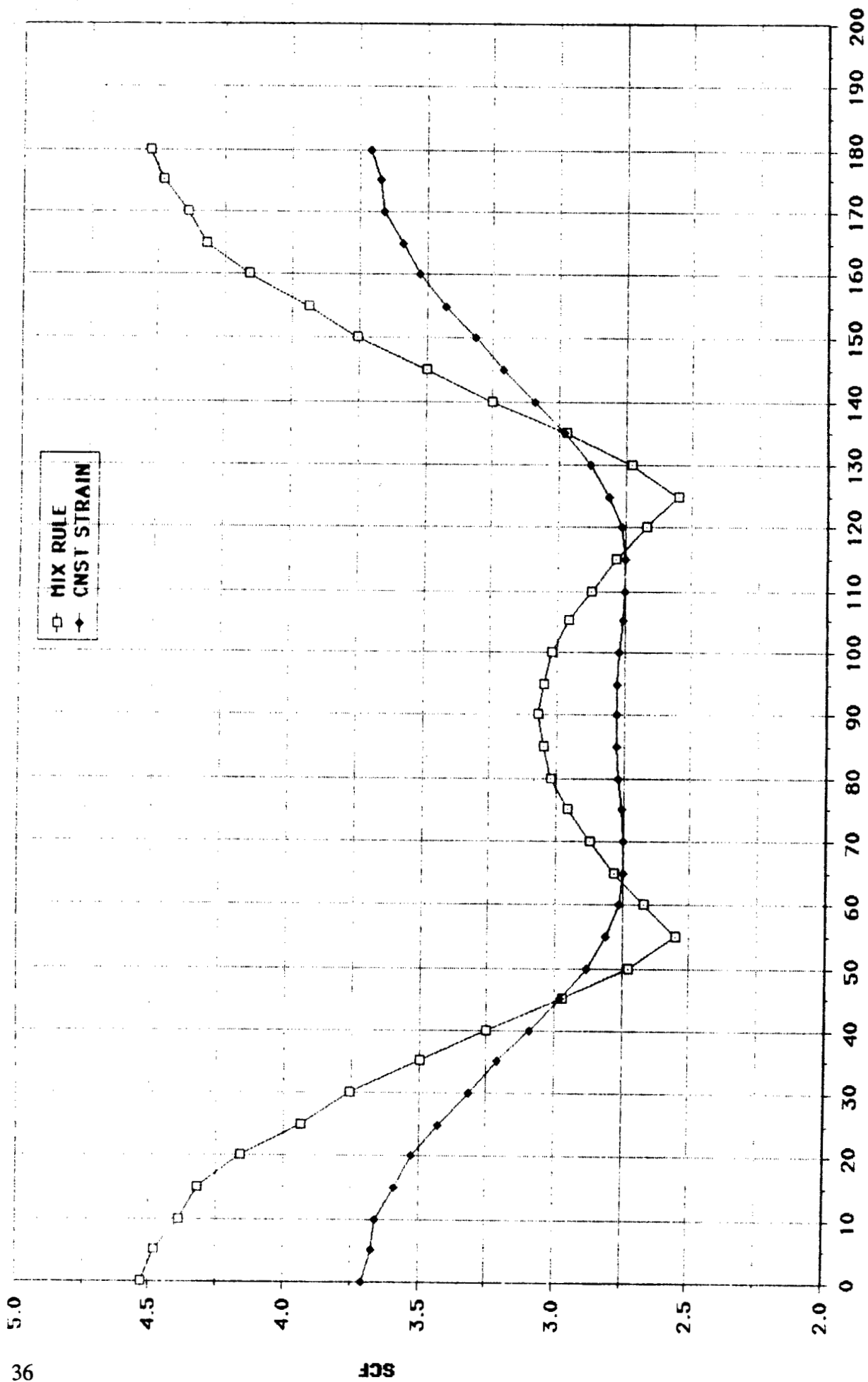


Figure 28. SCF maxima correlation, -60°F.



PHI (DEGREES)
 Figure 29. SCF maxima correlation, -60°F.

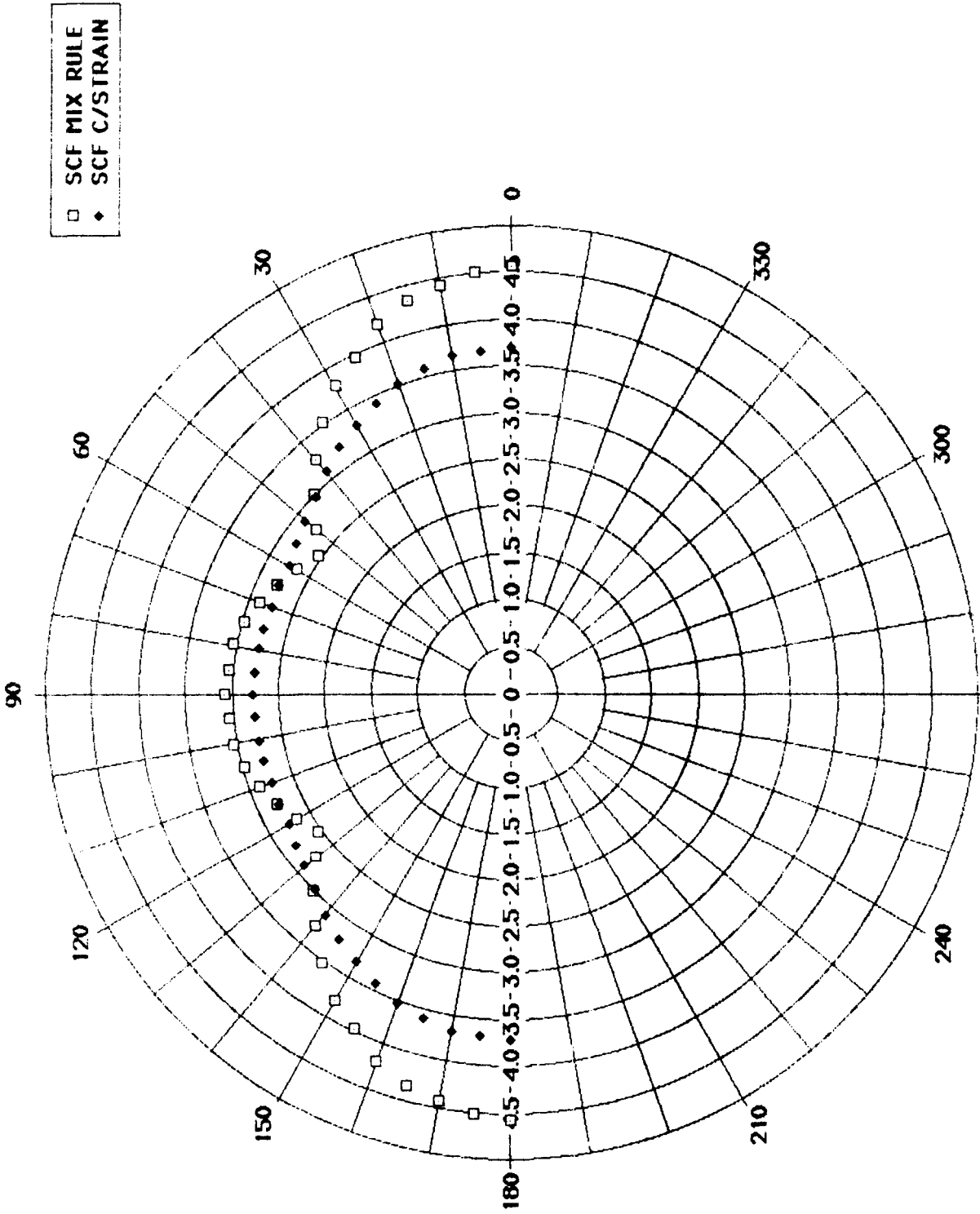
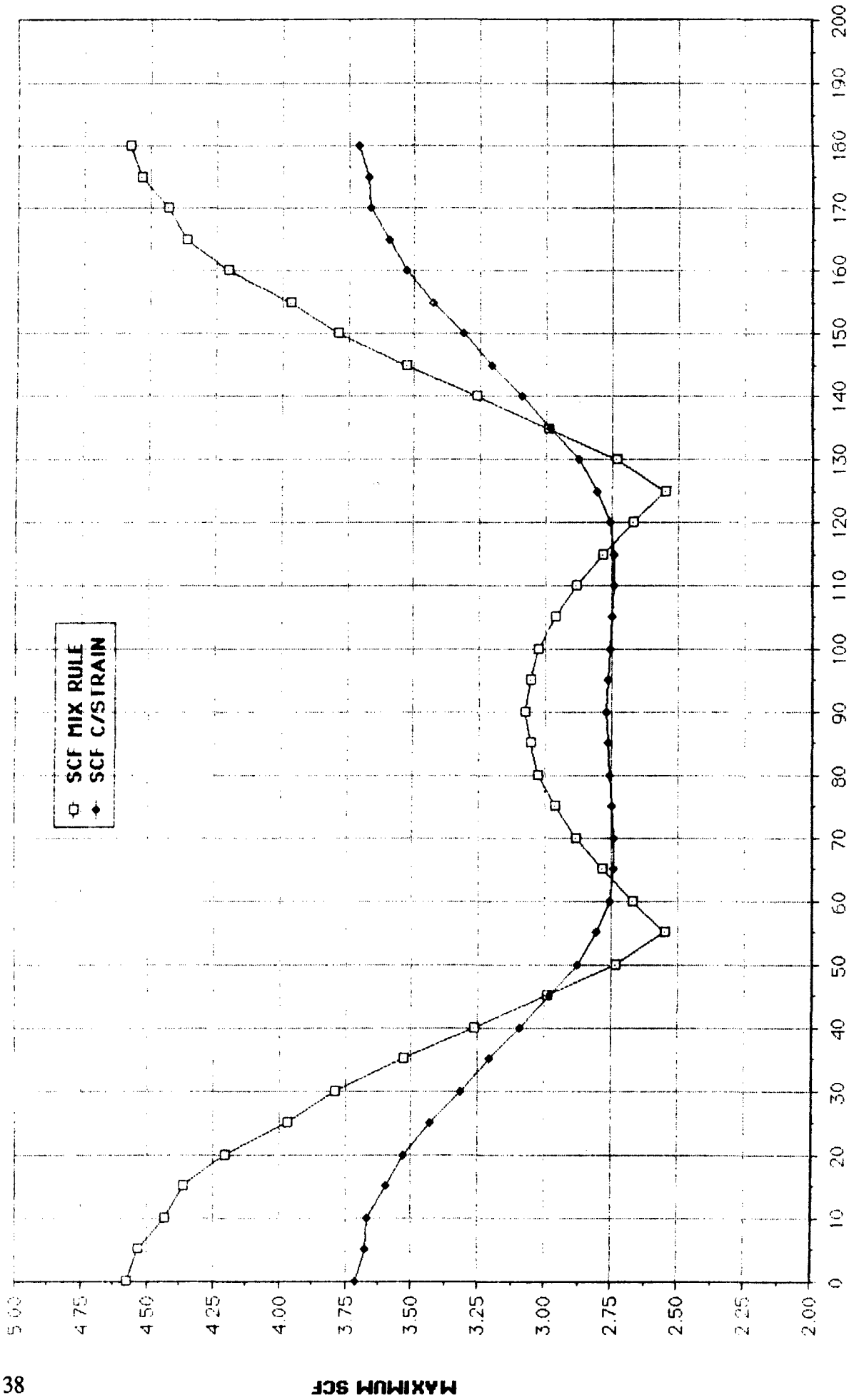


Figure 30. SCF maxima correlation, 70°F.



PHI (DEGREES)
 Figure 31. SCF maxima correlation, 70°F.

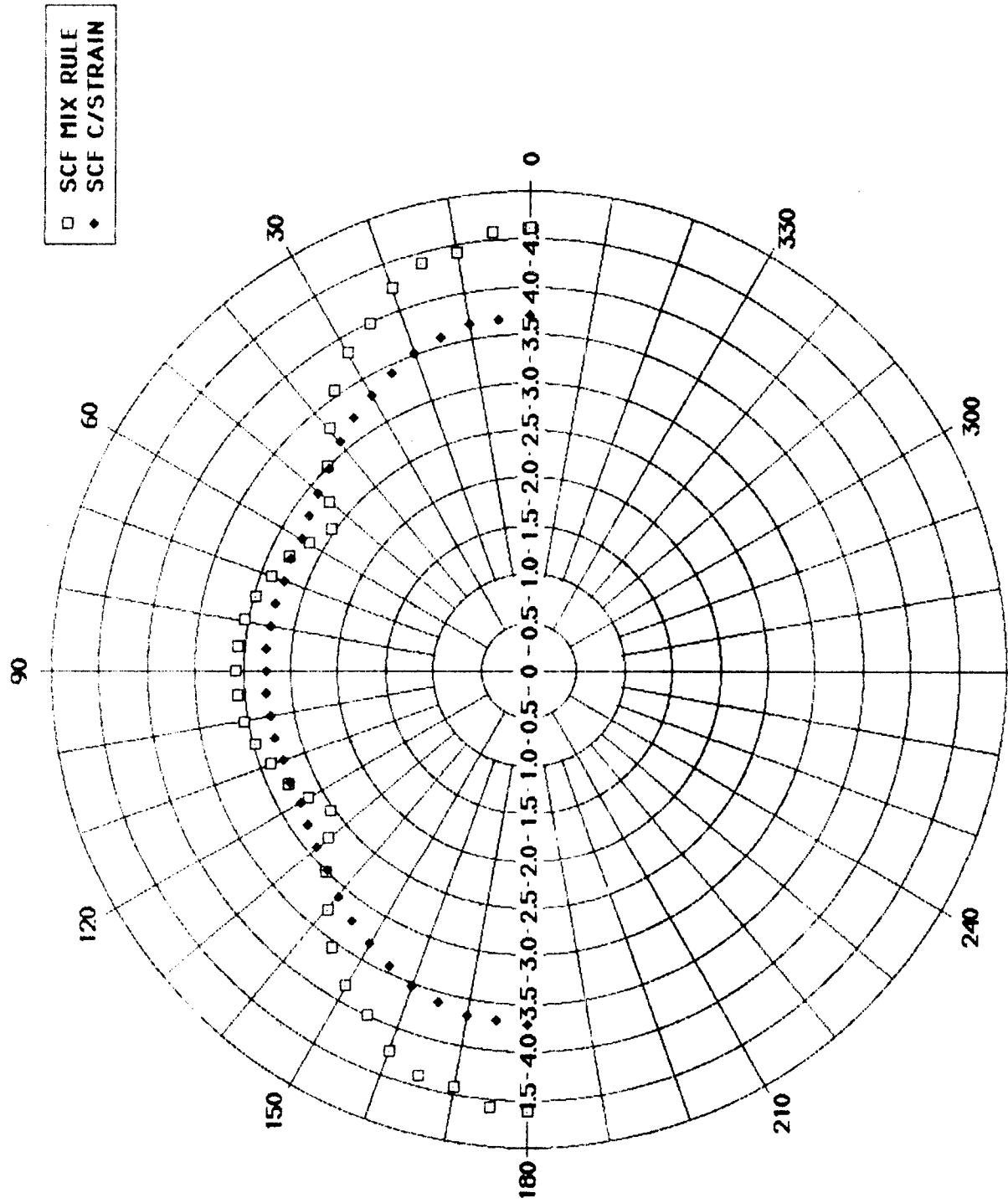
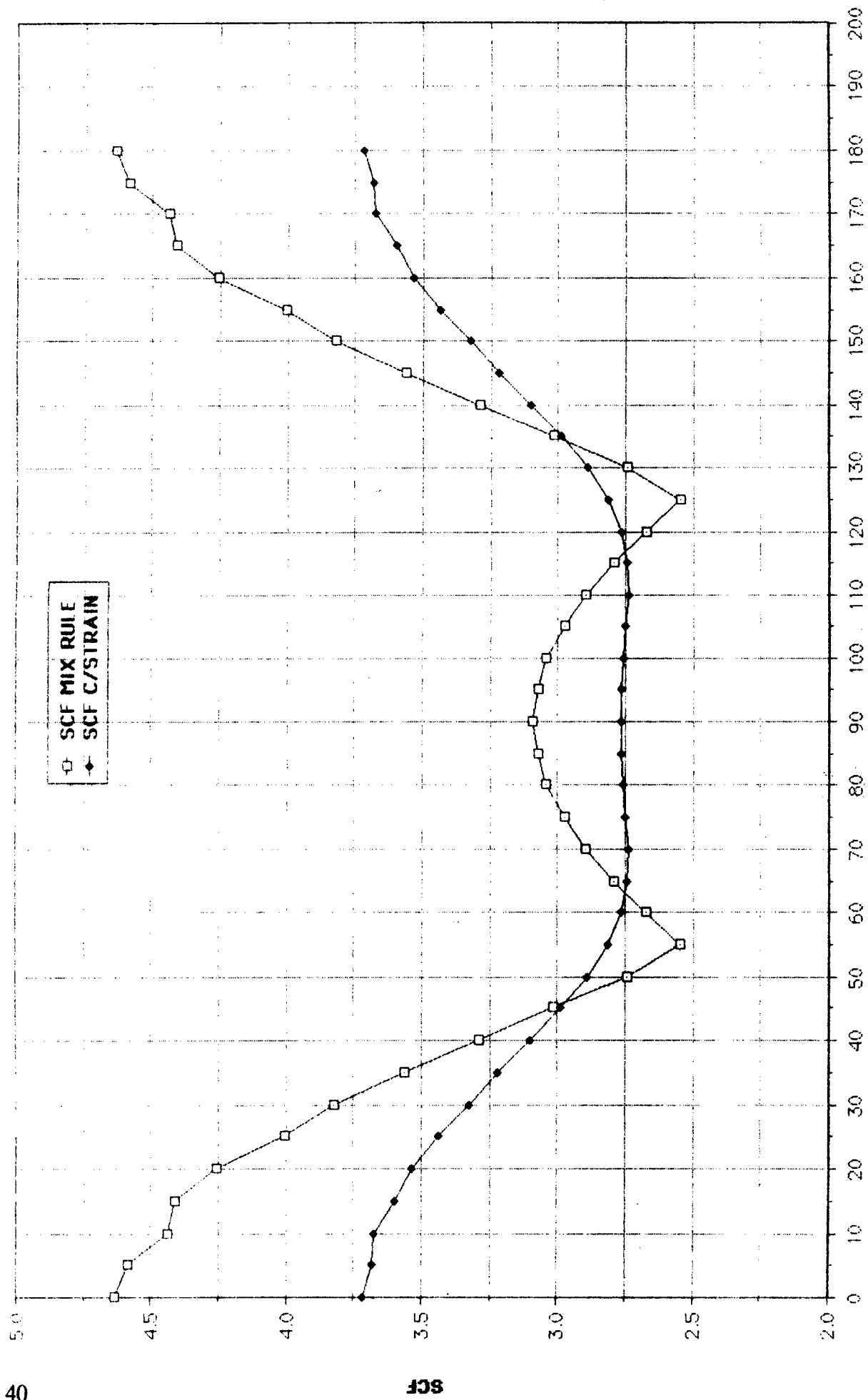


Figure 32. SCF maxima correlation, 200°F.



PHI (DEGREES)
 Figure 33. SCF maxima correlation, 200°F.

TABLE 1. STRESS CONCENTRATION FACTOR CORRELATION.

LOAD (LBS)	DATA FOR PHI=0° ALPHA=90°											
	-60° F				70° F				200° F			
	SCF EXPMT	SCF MIX RULE	SCF CNST STRAIN	SCF EXPMT	SCF MIX RULE	SCF CNST STRAIN	SCF EXPMT	SCF MIX RULE	SCF CNST STRAIN	SCF EXPMT	SCF MIX RULE	SCF CNST STRAIN
600	4.09	4.53	3.71	3.53	4.58	3.71	3.53	4.58	3.71	3.00	4.64	3.72
1000	4.36	4.53	3.71	3.71	4.58	3.71	3.71	4.58	3.71	3.22	4.64	3.72
2000	4.36	4.53	3.71	3.98	4.58	3.71	3.98	4.58	3.71	3.29	4.64	3.72
3000	4.36	4.53	3.71	3.88	4.58	3.71	3.88	4.58	3.71	3.39	4.64	3.72
4000	4.36	4.53	3.71	3.84	4.58	3.71	3.84	4.58	3.71	3.38	4.64	3.72



Report Documentation Page

1. Report No. NASA CR-179439		2. Government Accession No.		3. Recipient's Catalog No.	
4. Title and Subtitle Temperature Effect on Stress Concentration Around Circular Hole in a Composite Material Specimen Representative of X-29A Forward-Swept Wing Aircraft				5. Report Date August 1988	
				6. Performing Organization Code	
7. Author(s) Hsien-Yang Yeh				8. Performing Organization Report No. H-1514	
				10. Work Unit No. RTOP 533-02-5	
9. Performing Organization Name and Address NASA Ames Research Center Dryden Flight Research Facility P.O. Box 273, Edwards, CA 93523-5000				11. Contract or Grant No. NGT05020412	
				13. Type of Report and Period Covered Contractor Report	
12. Sponsoring Agency Name and Address National Aeronautics and Space Administration Washington, DC 20546				14. Sponsoring Agency Code	
				15. Supplementary Notes NASA Technical Monitor: William L. Ko, Ames Research Center, Dryden Flight Research Facility, Edwards, California 93523-5000	
16. Abstract The theory of anisotropic elasticity was used to evaluate the anisotropic stress concentration factors of a composite laminated plate containing a small circular hole. This advanced composite material was used to manufacture the X-29A forward-swept wing. Observe that the usual isotropic material stress concentration factor is three. It was found for composite material, that the anisotropic stress concentration factor is no longer a constant, and that the locations of maximum tangential stress points could shift by changing the fiber orientation with respect to the loading axis. The analysis showed that through the lamination process, the stress concentration factor could be reduced drastically, and therefore the structural performance could be improved. Both the mixture rule approach and the constant strain approach were used to calculate the stress concentration factor of room temperature. The results predicted by the mixture rule approach were about twenty percent deviate from the experimental data. However, the results predicted by the constant strain approach matched the testing data very well. This showed the importance of the inplane shear effect on the evaluation of stress concentration factor for the X-29A composite plate. At low temperature (-60 °F), the results predicted by the mixture rule approach provided good correlation with the experimental data. At elevated temperature (200 °F), the results calculated from the constant strain approach were about ten percent conservative than the experimental data. These showed both the advantages and the limitations of different analytical models in predicting stress concentration factors at various temperature levels. Furthermore, the experimental data showed the stress concentration factors decreased as the temperature increased.					
17. Key Words (Suggested by Author(s)) Composite plate Stress concentration Temperature			18. Distribution Statement Unclassified — Unlimited Subject category 39		
19. Security Classif. (of this report) Unclassified		20. Security Classif. (of this page) Unclassified		21. No. of pages 44	22. Price A03